Transport of Magnetic Helicity in Accretion Disks

Transport of Magnetic Helicity in Accretion Disks

By

Benjamin B. H. Jackel, B.Sc.

A Thesis
Submitted to the School of Graduate Studies
in Partial Fulfilment of the Requirements
for the Degree
Master of Science

McMaster University

MASTER OF SCIENCE (2010) McMaster University

(Physics and Astronomy) Hamilton, Ontario

TITLE: Transport of Magnetic Helicity in Accretion Disks

AUTHOR: Benjamin Jackel, B.Sc. (McMaster University)

SUPERVISOR: Ethan Vishniac

NUMBER OF PAGES: xiii, 71

Abstract

Astrophysical disks are found in many areas of astrophysics, from the protoplanetary disks in which planets are thought to be born, to the accretion disks around white dwarfs, merging stars, and black holes. The key to understanding these disks, is to understand how material overcomes the rotational support and acretes. Whatever mechanism is responsible must necessarily explain the transport of angular momentum outward.

The current mechanism used to explain this is the magnetorotational instability (MRI). Its ability to transport angular momentum as well as drive a magnetic dynamo, will be discussed in this thesis. The linear equations of motion for a locally Cartesian patch will be solved numerically to get the time evolution of the magnetic and velocity fields. From these solutions, quadratic quantities in the perturbation variables will be calculated, namely the angular momentum and magnetic helicity. The time evolution of these quantities can tell us about the MRI's ability to both transport angular momentum and drive a dynamo through magnetic helicity.

By solving the equations of motion in a locally Cartesian patch of a shearing disk, I have calculated the flux of angular momentum and magnetic helicity. The time evolution of these quantities shows that the ability to transport magnetic helicity is very similar the ability to transport angular momentum. This relation is true for a parameter space which corresponds to the asymptotic limit for the MRI.

Acknowledgements

I would first of all like to acknowledge my supervisor, Ethan Vishniac for his patience and support over the last two years. I am grateful to James Wadsley and Nicholas Kevlahan for their advice on the numerical methods used in this thesis. A special thanks to Leo van Nierop and Matt Minnick and all the other graduate students that I have harassed with questions about everything from fluid mechanics to tensor calculus. Finally, I thank my wife Margaret for keeping me at my current level of sanity during all of the frustrating debugging of code, scribbling of math and terrible grammar.

Dedicated to my wife Margaret and my Mom and Dad.

Table of Contents

List of Figures

List of Tables

Chapter 1

Introduction

The formation of a disk is ubiquitous in astrophysics. These disks, called accretion disks, play an important role in the formation of stars and planets as well as powering the centres of active galaxies. The accretion disk moderates how quickly material is accreted onto the central object as well as provide a mechanism for angular momentum to be transported from the inner to the outer region. An example is that young stars are observed to have rotation speeds much below break up speed which would be expected since the star forms out of a rotationally supported disk, thus a way to transfer the angular momentum outward is needed.

For a particle or, more generally, a fluid element to fall into the central object it must lose angular momentum. Conservation of angular momentum implies that this fluid element must give the lost angular momentum to another fluid element whose orbit will increase in radius.

To study the accretion disk we need to treat the disk material as a fluid so that we can use fluid dynamics to solve the equations of motion and deduce its properties. If the gas is assumed to be a fluid, the Rayleigh stability criterion given by $\frac{\partial(R^2\Omega)}{\partial R} > 0$, where Ω is the angular velocity and R is the radius, is equivalent to saying that angular momentum increase outward and that the a Keplerian disk should be hydrodynamically stable. If the fluid has a viscosity, it will heat up the fluid through friction and will then begin to radiate energy and angular momentum away. The first attempts using physical viscosity by Lynden-Bell & Pringle (1974), led to accretion rates which were too small by many orders of magnitude, thus a way to enhance this viscosity was needed. One way was to create an enhanced viscosity by using turbulence, an idea which, has been around since Prandtl and Boussinesq according to Frisch & Orszag (1990). Shakura & Sunyaev (1973) invoked turbulence to create an enhanced viscosity which led to a better fit to the observational data in their α-disk model. It was shown that hydrodynamic instabilities were not enough to make the disk turbulent. It is now widely accepted that the origin of turbulence in accretion disks is not hydrodynamic, but rather a linear magnetic instability as proposed by Balbus & Hawley (1991). This instability, named the magnetorotational instability (MRI), is an instability in a weakly magnetized disk which creates magnetohydrodynamic turbulence, transports angular momentum and powers a magnetic dynamo. Viscous heating and luminosity from the central object ionize the disk which is then highly conducting so that the magnetic field lines are frozen into and follow the dynamics of the fluid thus providing the conditions necessary for the MRI to function.

It is no surprise that magnetic fields should play an important factor in these types of astrophysical phenomena, Chandrasekhar (1960) and Velikhov (1959) separately theorized the MRI, though it was not applied to accretion disks until much later. The model proposed by Lynden-Bell & Pringle (1974) suggested that the turbulent effects should be much stronger than the magnetic effects. On the other hand, Shakura & Sunyaev (1973) hypothesized that the magnetic field could be an important effect, but did not produce a quantitative analysis. The MRI however, can arise from even an initially weak field, drive a magnetic dynamo, and enhance angular momentum transport via the magnetohydrodynamic turbulence.

With a magnetized disk that has been modelled as a fluid it is now possible to use the tools of magnetohydrodynamics to study accretion disks and more specifically the MRI. There are still many open questions about the MRI and the dynamo process tied to it such as the effects of magnetic buoyancy and the Parker instability (Tout & Pringle, 1992). Of theoretical importance is the role of magnetic helicity in the MRI and the dynamo process. It has been suggested by Vishniac (2009), that the MRI creates a magnetic helicity flux which drives the dynamo process. It is this hypothesis that I intend to study over the course of this thesis, focussing namely on the generation of magnetic helicity flux by an MRI using numerical methods.

The transport of angular momentum is the other long standing question about accretion disks and will be compared to the magnetic helicity flux from this calculation. The goal is to understand how the efficiency of the magnetic helicity transport compares to the efficiency of the angular momentum transport in an accretion disk. The magnetic helicity transport gives us an understanding as to how efficient the dynamo is and together with the angular momentum describe how important the MRI is to the accretion disk.

Chapter 2

Background

2.1 Fluid Mechanics

To study accretion disks we can treat the gas and dust that makes up the accretion disk as a fluid. The mathematical framework used to describe fluids and how they move is called Fluid Mechanics. Fluid mechanics is a continuum theory, which means that it can not be used to describe an individual particle, rather it must treat the system as a continuous fluid. To this end, the fluid must be highly collisional or have a small mean free path compared to the size of the system.

The set of equations which are used to describe the motion of a fluid and the forces involved, are called the Navier Stokes equations, with the case of an incompressible fluid given by equation (2.1) (Chorin & Marsden (1979)). Here, $\mathbf{u}$ is the velocity of a fluid element, p is the pressure, ρ is the density and ν is the kinematic viscosity.

$$\frac{\partial \mathbf{u}}{\partial t} + \mathbf{u} \cdot \nabla \mathbf{u} = -\frac{1}{\rho} \nabla p + \nu \nabla^2 \mathbf{u} \tag{2.1}$$

$$\nabla \cdot \mathbf{u} = 0 \tag{2.2}$$

The last term of equation (2.1) is perhaps the most relevant to the discussion since it is the term which is responsible for diffusion and loss of energy and thus angular momentum in the disk. Also relevant to the discussion is the dimensionless Reynolds number, Re. The Reynolds number describes the ratio of the inertial to viscous forces and is defined as $Re = \frac{VL}{\nu}$, where L is a characteristic length scale of the system (disk height in an accretion disk), and V is the mean velocity of the fluid. When the Reynolds number is small, the fluid flow is laminar, whereas it generally becomes turbulent at high Reynolds numbers. This is important since many astrophysical fluids are observed to have very high Reynolds numbers.

If there are additional forces at work, such as gravity, there is an additional term to (2.1) to account for this. The part of the disk being looked at will have a vertical length scale much shorter than the pressure scale height, so that gravity will not contribute to the dynamics. This term will also be dropped when the MHD equations are introduced in the next section so that buoyancy effects are small and the fluid can be treated as incompressible.

2.2 Magnetohydrodynamics

The motivation behind magnetohydrodynamics (MHD) is to include the forces involved in electromagnetism with the forces of fluid mechanics. Accretion disks are generally observed to be in a plasma state which satisfies the criterion that the fluid is highly conducting.

The equations which describe E&M are condensed in Maxwell's equations, given by equations (2.3) plus the Lorentz force equation, $\mathbf{F} = q\mathbf{E} + q(\mathbf{v} \times \mathbf{B})$. Here $\mathbf{E}$ is the electric field, $\mathbf{B}$ is the magnetic field, c is the speed of light, ρ is the charge density, and $\mathbf{J}$ is the current density. Of special note is equation (2.3c), which is Faraday's law of induction and will play a special role in the formulation of the MHD equations.

$$\nabla \cdot \mathbf{E} = 4\pi\rho \tag{2.3a}$$

$$\nabla \cdot \mathbf{B} = 0 \tag{2.3b}$$

$$\nabla \times \mathbf{E} + \frac{1}{c}\frac{\partial \mathbf{B}}{\partial t} = 0 \tag{2.3c}$$

$$\nabla \times \mathbf{B} - \frac{1}{c}\frac{\partial \mathbf{E}}{\partial t} = \frac{4\pi}{c}\mathbf{J} \tag{2.3d}$$

In the non-relativistic limit, the displacement current can be dropped. In the presence of light charge carriers the Lorentz force vanishes in the frame of the fluid so that $\mathbf{E} + (\mathbf{v} \times \mathbf{b}) = 0$. In this limit, the field lines will become frozen into the fluid and so the dynamics will be functions of both the magnetic field and the momentum of the fluid. To this end, the Navier-Stokes equations along with the E&M forces provide the basis of the MHD equations

$$\rho(\frac{\partial \mathbf{u}}{\partial t} + \mathbf{u} \cdot \nabla \mathbf{u}) = -\nabla p + \mathbf{j} \times \mathbf{B} - \rho \nabla \phi_g, \tag{2.4a}$$

$$\frac{\partial \mathbf{B}}{\partial t} = \nabla \times (\mathbf{u} \times \mathbf{B}), \tag{2.4b}$$

$$\frac{\partial \rho}{\partial t} + \nabla \cdot \rho \mathbf{u} = 0, \tag{2.4c}$$

$$\nabla \cdot \mathbf{u} = 0. \tag{2.4d}$$

Here, $\mathbf{u}$ is the velocity field, $\mathbf{B}$ is the magnetic field, $\mathbf{j}$ is the current density, and ρ is the mass density. Equation (2.4a) describes the momentum of the fluid, equation (2.4b) is Faraday's induction equation, equation (2.4c) is the continuity equation, and equation (2.4d) enforces the incompressibility of the fluid.

With these tools in place, a quantity called the magnetic helicity may be defined. The magnetic helicity

$$H = \int \mathbf{A} \cdot \mathbf{B} \, d^3\mathbf{r}, \tag{2.5}$$

is a measure of the "twistedness" of the magnetic field, and is directly analogous to the fluid helicity in fluid mechanics. An important property of the magnetic helicity is that it is a conserved quantity even for an infinitesimal resistivity. Also, it is gauge-dependant due to the presence of the vector potential, $\mathbf{A}$. This quantity turns out to be especially important for driving the dynamo which is discussed in the next section. This is because its flux provides a term which is parallel to the large scale magnetic field, a property which is required to complete the regenerative cycle in the dynamo.

The vector potential is given by

$$\nabla^2 \mathbf{A} = -\mathbf{J}, \tag{2.6}$$

and the gauge, which will be assumed, is the one in which the current helicity and magnetic helicity are closely connected in space.

$$\mathbf{A} = \int \frac{\mathbf{J}(\mathbf{x}')}{4\pi|\mathbf{x} - \mathbf{x}'|} d^3\mathbf{x}', \tag{2.7}$$

that is, the Coulomb Gauge.

The scalar potential will also be used and is given by equation (2.8).

$$\nabla^2 \phi = -4\pi\rho \tag{2.8}$$

The MHD equations give rise to wave solutions, much like the equations of fluid mechanics do. In MHD there are 3 additional waves, compared to the 1 in fluid mechanics. In fluid mechanics a characteristic speed appears called the sound speed, c_s. In MHD the characteristic speed for transverse waves is the Alfvén speed, V_A. The Alfvén speed is defined as $V_A = \frac{B_0}{\sqrt{\rho}}$, where B_0 is the magnetic field strength, and ρ is the density of the fluid, (Biskamp, 1993).

2.3 Magnetic Dynamos

The first use of the word dynamo applied to devices which generated electric current through application of Faraday's law. The word was eventually used to describe the physical process by which a magnetic field is generated and maintained from an initial field. It is from this word and definition in which dynamo theory comes from. The motivation behind dynamo theory is to describe the generation of magnetic fields. The Earth's magnetic field and the solar magnetic field were the driving forces behind the formulation of dynamo theory. Magnetic dynamo can be found from laboratory scales all the way up to a galactic scale. The dynamo I will be discussing are of an astrophysical context, with a size on the order of the accretion disk being simulated.

The types of dynamo theories that are applied to astrophysical situations generally fall under the category of mean field theories. This means that the problem can be broken into a large scale and small scale, where the large scale is generated from the average or mean of the fluctuating small scale field. For example,

$$\mathbf{B}_T = \mathbf{B} + \mathbf{b},$$

$$\langle \mathbf{b} \rangle = 0.$$

The key equation in magnetic dynamo theory is the Induction Equation,

$$\frac{\partial \mathbf{B}}{\partial t} = \eta \nabla^2 \mathbf{B} + \nabla \times (\mathbf{V}_T \times \mathbf{B}_T), \tag{2.9}$$

The first term on the right hand side describes the magnetic diffusion, where η is the magnetic diffusivity, the second term is the induction equation. The relative strengths of the second term to the first term gives the magnetic Reynolds number, which is analogous to the Reynolds number in fluid mechanics.

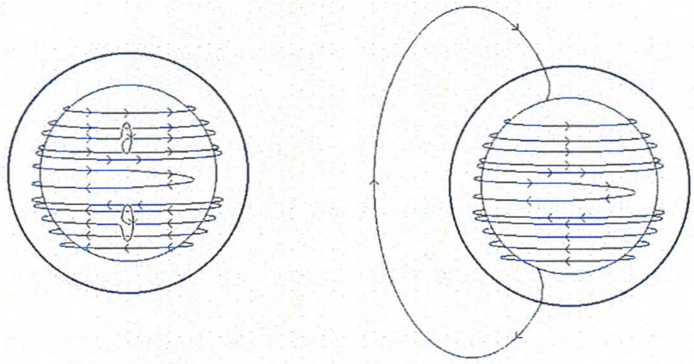

Figure 2.1: The alpha effect, shown on the left, describes how a poloidal field might be created from a toroidal field. If the fluid has a non-zero helicity and also some buoyancy or turbulent motion, then the magnetic field might develop a loop oriented in the same direction as the initial poloidal field. Reconnection can then join the loops to regenerate the initially poloidal field and set the conditions for the ω effect. The ω effect on the right is the other half of the $\alpha - \omega$ dynamo. The result of a differential rotation is to drag the field lines with the fluid creating a toroidal field from the initial poloidal state. http://solarscience.msfc.nasa.gov/dynamo.shtml

An important concept in a dynamo is where the motion of the fluid provides a mechanism to regenerate or grow the initial magnetic field. One way to do this is the α effect. If the mean electromotive force can be written as

$$\mathcal{E} \equiv \langle \mathbf{u} \times \mathbf{b} \rangle \,, \tag{2.10}$$

then $\mathcal{E}$ can be expanded in a series with the first term given by

$$\mathcal{E}_i^{(0)} = \alpha_{ij} B_{0j} \tag{2.11}$$

(Parker, 1970). Here, $\mathcal{E}$ is the electromotive force, B_{0j} is the component of the large scale magnetic field. The term α_{ij} is a pseudo-tensor whose trace is the current helicity and fluid helicity, and when multiplied by a turbulence correlation time (τ_c) is the current helicity tensor minus the fluid helicity tensor.

It is this term that allows for a toroidal field to be generated from a poloidal one, which will be turned back into a toroidal field by the next step. This next step is called the ω effect, since it is caused by differential rotation. The ω effect is simply described by the action of differential rotation on the magnetic field lines. Since the field lines are frozen into the fluid they get dragged around with the fluid, and so an originally poloidal field will be stretched and dragged into a toroidal configuration. The α and ω effects are perhaps best described by a diagram, such as figure 2.1. These two effects are the basis of the $\alpha - \omega$ dynamo which is primarily used to describe the geo and solar magnetic fields.

There are some problems with this model arising from the conservation of magnetic helicity. The part of the magnetic helicity coming from small scale motions is defined as $h = \langle \mathbf{a} \cdot \mathbf{b} \rangle$. The conservation of this quantity implies that there will be an accumulation of h which will poison the dynamo through its contribution to the resulting current helicity and the α effect. The time evolution of h from Vishniac & Cho (2001) is,

$$\partial_t h = -\nabla \cdot \mathbf{J}_H - 2\mathbf{B} \cdot \langle \mathbf{v} \times \mathbf{b} \rangle, \tag{2.12}$$

where $\mathbf{J}_H$ is the anomalous magnetic helicity and the second term on the right hand side describes the transfer of h to the large scale component of the magnetic helicity. The left hand side will be forced to be small by this effect so that the $\langle \mathbf{v} \times \mathbf{b} \rangle$ term will be proportional to the divergence of the magnetic helicity flux. With this definition we may rewrite equation (2.10) as

$$\mathcal{E} = \mathcal{E}_{\perp} - \frac{\mathbf{B}}{2B^2} \nabla \cdot \mathbf{J}_H, \tag{2.13}$$

where $\mathcal{E}_{\perp}$ is the component of the electromotive force which is perpendicular to the large scale magnetic field.

The key point here is that there is a component of the magnetic helicity current which is parallel to the large scale magnetic field which is exactly what is needed to drive a dynamo. Thus, a way to generate a magnetic helicity flux would also power a dynamo. For the generation of magnetic helicity on eddy scales we look to the magnetorotational instability.

2.4 The Magnetorotational Instability

The magnetorotational instability (MRI) plays a central role in accretion disks for the transport of angular momentum, generation of magnetohydrodynamic turbulence and the magnetic helicity flux to drive the magnetic dynamo.

A fluid element which is perturbed outward will fall behind the fluid elements it is connected to by the embedded magnetic field. This leads to an acceleration of the perturbed element, transferring angular momentum to it and causing it to continue to move outward.

The concepts and theory for the MRI have been around since Chandrasekhar (1960) and Velikhov (1959), but the first application to an accretion disk was done by Balbus & Hawley (1991). The original work and the work by Balbus

& Hawley (1991) assume an external vertical field and indeed the description of the MRI given above is for a vertical field. In the context of studying the dynamo, starting with an internally generated, large scale azimuthal field will be more relevant (Vishniac & Diamond (1992)).

In the case where the large scale magnetic field is azimuthal or $\mathbf{B} = B_\phi \hat{\boldsymbol{\phi}}$, and including the Keplerian shear $\mathbf{V} = r\Omega(r)\hat{\boldsymbol{\phi}}$, the governing linear equations of motion are given by equations (2.14) from Vishniac & Diamond (1992),

$$\mathbf{b} = B_\phi \frac{m}{r\bar{\omega}}\mathbf{u} + iB_\phi \frac{3\Omega m}{2\bar{\omega}^2 r} u_r \hat{\boldsymbol{\phi}}, \tag{2.14a}$$

$$i\bar{\omega} u_r = 2\Omega u_\phi - \partial_r \psi + V_A(ik_y b_r - \partial_r b_\phi), \tag{2.14b}$$

$$i\bar{\omega} = -\frac{\Omega}{2} u_r - ik_y \psi, \tag{2.14c}$$

$$i\bar{\omega} = ik_z \psi + V_A(ik_y b_z - ik_z b_\phi). \tag{2.14d}$$

Here, k_r, k_ϕ, and k_z are wavenumbers with $\frac{m}{r} = k_\phi$, Ω is the angular frequency of the disk, $\bar{\omega}$ is the comoving frequency, V_A is the Alfvén velocity, and ψ is the pressure.

The dispersion relation is then,

$$\left[1 - \frac{k_z^2}{k_*^2}\frac{\Omega^2}{\tilde{\omega}^2}\left(1 + 4\frac{\omega_A^2}{\tilde{\omega}}\right) + \frac{9}{2}\frac{(m/r)^2 \omega_A^2 \Omega^2}{k_*^2(\tilde{\omega}^2 + \omega_A^2)\tilde{\omega}^2}\right] u_r - \frac{1}{k_*^2}\partial_r^2 u_r = -3\frac{\omega_A^2}{\tilde{\omega}^2}\frac{\Omega}{\bar{\omega}}\frac{m}{rk_*^2}\partial_r u_r$$

where $k_*^2 = k_z^2 + (m/r)^2$, $\tilde{\omega}^2 = \bar{\omega}^2 - \omega_A^2$, $\omega_A = \frac{m}{r}V_A$ and $\nabla \cdot \mathbf{u} = 0$ have been used. Finally, this dispersion relation can be reduced to

$$\tilde{\omega}^6 + \tilde{\omega}^4(\omega_A^2 - \omega_I^2) + \tilde{\omega}^2(-5\omega_A^2\omega_I^2 + \frac{9}{2}\frac{(m/r)^2}{k^2}\omega_A^2\Omega^2) - 4\omega_I^2\omega_A^4 = 0,$$

with $\omega_I^2 = \frac{k_z^2}{k^2}\Omega^2$ and k is the total wavenumber.

In the limit of large radial wavenumbers, the above dispersion relation reduces to that of the MRI dispersion relation quoted in Balbus & Hawley (1991),

$$\tilde{\omega}^4+\frac{k_z^2}{k^2}\left[\frac{3}{5\rho}\left(\frac{k_R}{k_z}\frac{\partial P}{\partial z}-\frac{\partial P}{\partial R}\right)\left(\frac{k_R}{k_z}\frac{\partial \ln P\rho^{-5/3}}{\partial z}-\frac{\partial \ln P\rho^{-5/3}}{\partial R}\right)-\kappa^2\right]\tilde{\omega}^2-4\Omega^2\frac{k_z^4 v_{Az}^2}{k^2}=0.$$

An important result from this MRI dispersion relation is the growth rate of the perturbed magnetic field $\sqrt{3}k_\phi V_A$ when k_ϕ is small, and will grow for k_z/k_ϕ e-foldings. These predictions will provide test cases for numerical solver that will be employed in chapter 4.

2.5 Accretion Disks

The key question surrounding accretion disks is how do they transport angular momentum away from the central mass? If a disk can be treated as a fluid undergoing Keplerian rotation so that $\Omega \sim R^{-3/2}$, then it should be hydrodynamically stable. More generally, a disk will be stable if $\frac{\partial(R^2\Omega)}{\partial R} > 0$, where Ω is the angular velocity and R is the radius. This inequality is known as the Rayleigh Stability Criterion and is automatically satisfied for a Keplerian disk. If, on the other hand, the disk has a magnetic field threaded through it, it will be subject to a new stability criterion, $\frac{\partial\Omega^2}{\partial R}$. A Keplerian disk will almost never satisfy this criterion and so should be unstable.

If the fluid in the disk has a viscosity, then differential rotation will lead to energy being radiated away from this disk through viscous heating. To reach the observed accretion rates, the viscosity must be orders of magnitude higher than estimates from microphysical processes.

Shakura & Sunyaev (1973) put forth an empirical model using turbulence as a way to artificially enhance the viscosity in the so called α disk model. The enhanced viscosity is parametrized by $\nu_t = \alpha_{ss} c_s H$ where ν_t is a turbulent viscosity, c_s is the sound speed in the fluid and H is the scale height of the disk. The standard α model suggests that a typical accretion disk should be hydrodynamically unstable corresponding to an α_{ss} of order unity.

Although the α prescription remains a popular way to approximate disk behaviour, some caution must be taken. While it is normally the case that a high Reynolds number means turbulence and thus enhanced transport, the presence of epicycles leads to there being no enhanced transport and so a turbulent disk should be hydrodynamically stable (Balbus et al., 1996). This is not the end of the α prescription though, if the turbulence is magnetohydrodynamic it could still cause an enhanced viscosity and make the disk unstable.

Chapter 3

Methodology

The goal is to calculate the magnetic helicity flux and angular momentum flux caused by the MRI in an accretion disk. The first step is to start at the large scale accretion disk level. That is, there is a disk with a rotation velocity, $\mathbf{V} = r\Omega\hat{\boldsymbol{\phi}}$ and an azimuthal magnetic field, $\mathbf{B} = V_A\hat{\boldsymbol{\phi}}$. The coordinate system is cylindrical with V_A as the Alfvén speed and Ω is the angular velocity. To calculate the magnetic helicity flux from the MRI we must look at a small patch of the accretion disk to study the behaviour of the velocity and magnetic fields on that scale. In this small patch the fluid will be incompressible with a scale height much smaller than the pressure scale height. In this way vertical gravity will not enter the dynamics, and the effects of buoyancy will be small so that we may focus on the generation of magnetic helicity. The large scale fields, $\mathbf{V}$ and $\mathbf{B}$ are to be considered background fields, while in this small patch we will consider $\mathbf{u}$ and $\mathbf{b}$ as the small scale velocity and magnetic fields. In general, capital letters will denote the large scale while lower case will denote the small scale quantities such that $\mathbf{B}_T = \mathbf{B} + \mathbf{b}$, and $\langle \mathbf{b} \rangle = 0$.

3.1 Equations of motion

While it is natural to work in cylindrical coordinates for the large scale fields, the local patch can be considered to have a radial length scale much larger than any other scale of interest so that the curvature effects can be neglected and we can work in Cartesian coordinates. It is this local patch which the dynamics of the MRI will be worked out and the magnetic helicity will be calculated from.

First, start with the linear equations of motion in this small patch with equations (2.14) from §2.4. Note that wavenumbers for k_ϕ and k_z have been defined, while a radial wavenumber has not. This is because a radial wavenumber would evolve in time and so it is left out. That is, the azimuthal and vertical directions are in Fourier space, while the radial part is in real space. To simplify these equations, $4\pi\rho = 1$ so that the magnetic field is a velocity, V_A and ψ become a pressure, Q. With these changes 2.4 can be transformed into,

$$\left(\partial_t - ik_y\frac{3}{2}\Omega x\right)\mathbf{b} = -\frac{3}{2}\Omega b_x\hat{\mathbf{y}} + ik_yV_A\mathbf{u}, \tag{3.1a}$$

$$\left(\partial_t - ik_y\frac{3}{2}\Omega x\right)\mathbf{u} = 2\Omega u_y\hat{\mathbf{x}} - \frac{1}{2}\Omega u_x\hat{\mathbf{y}} - \nabla Q + ik_yV_A\mathbf{b}, \tag{3.1b}$$

$$\nabla\cdot u = 0. \tag{3.1c}$$

These equations then need to be put into dimensionless units, so that they are conducive to solving with numerical methods. The scaling is such that time is in units of $\frac{1}{k_yV_A}$, x (radial distance) is in units of $\frac{2}{3}\frac{V_A}{\Omega}$, velocity in units of V_A, and Q in units of V_A^2.

With the units in place, we can define $\bar{\omega}_A \equiv \frac{k_y V_A}{\Omega}$ and $\kappa \equiv \frac{k_y}{k_z}$, so that equations (3.1a)-(3.2c) can be recast as

$$(\partial_t - ix)\,\mathbf{b} = -\frac{3}{2\bar{\omega}_A} b_x \hat{\mathbf{y}} + i\mathbf{u}, \tag{3.2a}$$

$$(\partial_t - ix)\,\mathbf{u} = \frac{2}{\bar{\omega}_A} u_y \hat{\mathbf{x}} - \frac{1}{2\bar{\omega}_A} u_x \hat{\mathbf{y}} - \frac{3}{2\bar{\omega}_A} \partial_x Q \hat{\mathbf{x}} - iQ\hat{\mathbf{y}} - \frac{i}{\kappa} Q\hat{\mathbf{z}} + i\mathbf{b}, \tag{3.2b}$$

$$\frac{3}{2}\partial_x u_x + i\bar{\omega}_A u_y + \frac{i\bar{\omega}_A}{\kappa} = 0. \tag{3.2c}$$

3.2 Projection Method

To solve (3.1a)-(3.1c), a method laid out by Chorin (1967) is used called the projection method. The method is formally described by Helmholtz-Hodge decomposition where the solenoidal and irrotational parts of a vector are separated. Alternatively, the incompressible part is mapped or projected onto the compressible solution and thus enforcing the incompressibility of the fluid. The relevant equation to work with is equation (3.2b), and will be rewritten as

$$\partial_t \mathbf{u} = RHS - \nabla Q$$

where RHS has absorbed $ix\mathbf{u} + i\mathbf{b} 2\Omega u_y \hat{\mathbf{x}} - \frac{1}{2}\Omega u_x \hat{\mathbf{y}}$. The next step, is to discretize this equation according to a first order finite difference method. Even though the method I will use is not a first order finite difference method, this example is illustrative of the actual technique used. After discretizing,

$$\frac{\mathbf{u}^{n+1} - \mathbf{u}^n}{dt} = RHS^n - \nabla Q^n$$

where n represents the number of timesteps.

The discretized equation is then split into two parts,

$$\mathbf{u}^* = \mathbf{u}^n + dt(RHS^n), \tag{3.3}$$

and

$$\mathbf{u}^{n+1} = \mathbf{u}^* - dt(\nabla Q). \tag{3.4}$$

The first step then, is to calculate the intermediate timestep, $\mathbf{u}^*$, from equation (3.3). This can be done by any numerical ordinary differential equations solver (in this case, a fourth order Runge-Kutta scheme).

The correction step is done by enforcing the divergence free condition, and is carried out by taking the divergence of equation (3.4) giving,

$$\frac{\nabla \cdot \mathbf{u}^*}{dt} = \nabla^2 Q, \tag{3.5}$$

and solving this equation. The result is then substituted into equation (3.4) to give the corrected timestep, $\mathbf{u}^{n+1}$.

To summarize this process,

1. Calculate the intermediate timestep $\mathbf{u}^*$ using eq. (3.3)

2. Calculate the pressure correction from eq. (3.5)

3. Correct $\mathbf{u}^*$ with the updated pressure with eq. (3.4)

Where the process diverges slightly from the standard projection method, is in the second step. The pressure correction is calculated by taking the divergence of equation (3.2b) to arrive at

$$\nabla^2 Q = \frac{2}{\bar{\omega}_A}\partial_x u_y - \frac{1}{2\bar{\omega}_A}\partial_y u_x + \frac{3}{2} i u_x,$$

using $\nabla \cdot \mathbf{u} = 0$.

In the normalized units, $\nabla \equiv (\frac{3}{2}\partial_x, i\bar{\omega}_A, \frac{i\bar{\omega}_A}{\kappa})$ and so the equation for Q becomes

$$\frac{\partial^2 Q}{\partial x^2} - K^2 Q = \frac{4}{3}\partial_x u_y + \frac{4}{9} i\bar{\omega}_A u_x, \tag{3.6}$$

where $K = \frac{2}{3}\bar{\omega}_A\sqrt{1+\frac{1}{\kappa^2}}$. The third step is followed as normal.

3.3 Magnetic Helicity

At each timestep the magnetic helicity current, $\mathbf{J}_H$, needs to be calculated according to

$$\mathbf{J}_H \equiv \mathbf{A} \times (\mathbf{u} \times \mathbf{B}) + \mathbf{B}\varphi, \tag{3.7}$$

where φ is the scalar potential, and $\mathbf{A}$ is the large scale vector potential.

The contribution to the helicity current due to small scale motions, $\mathbf{j}_h$, is the quantity of interest and follows the derivation by Vishniac & Cho (2001), except that there is the addition of a term from the large scale background velocity. Combining these gives

$$\mathbf{j}_h + \Delta\mathbf{j}_h,$$

where

$$\mathbf{j}_h = (\mathbf{a}\cdot\mathbf{B})\mathbf{u} + \mathbf{b}\varphi - \mathbf{B}(\mathbf{a}\cdot\mathbf{u}),$$

and

$$\Delta\mathbf{j}_h = (\mathbf{a}\cdot\mathbf{b})\mathbf{V} - \mathbf{b}(\mathbf{a}\cdot\mathbf{V}) + \mathbf{b}\Delta\varphi.$$

The small scale vector potential with the gauge such that

$$\mathbf{a} = \int \frac{\mathbf{j}(\mathbf{x}')}{4\pi|\mathbf{x}-\mathbf{x}'|}\, d^3\mathbf{x}',$$

is calculated from

$$\nabla^2 \mathbf{a} = -\mathbf{j}.$$

The scalar potential is the combination of the large scale fields with the small scale fields, given by

$$\varphi(\mathbf{x}) = -\int \frac{\nabla\cdot(\mathbf{u}(\mathbf{x}+\mathbf{x}')\times\mathbf{B}(\mathbf{x}+\mathbf{x}'))}{4\pi|\mathbf{x}'|}\, d^3x',$$

and

$$\Delta\varphi(\mathbf{x}) = -\int \frac{\nabla\cdot(\mathbf{V}(\mathbf{x}+\mathbf{x}')\times\mathbf{b}(\mathbf{x}+\mathbf{x}'))}{4\pi|\mathbf{x}'|}\, d^3x'.$$

The terms which are aligned with the large scale fields, $\mathbf{B}(\mathbf{a}\cdot\mathbf{u})$ and $(\mathbf{a}\cdot\mathbf{b})\mathbf{V}$, can be ignored since they do not contribute to $\nabla\cdot\mathbf{j}_h$. That is to say, they simply move the magnetic helicity in the azimuthal direction in the disk. The last two terms of $\mathbf{j}_h$ combine to give

$$\mathbf{b}(\Delta\varphi - \mathbf{a}\cdot\mathbf{V}) = \mathbf{b}(\mathbf{x})\int \frac{d^3x'}{4\pi|\mathbf{x}'|}\left(-\mathbf{b}(\mathbf{x}+\mathbf{x}')\cdot(\nabla\times\mathbf{V}) + \mathbf{j}(\mathbf{x}+\mathbf{x}')\cdot(\mathbf{V}(\mathbf{x}+\mathbf{x}')-\mathbf{V}(\mathbf{x}))\right).$$

Finally, this can be rewritten as

$$\mathbf{b}(\Delta\varphi - \mathbf{a}\cdot\mathbf{V}) = -\mathbf{b}(\mathbf{x})\int \frac{d^3x'}{4\pi}\left(\partial_k j_i(\mathbf{x}-\mathbf{x}')\right)|\mathbf{x}'|S_{ij}$$

by using integration by parts and

$$\mathbf{V}(\mathbf{x}+\mathbf{x}') - \mathbf{V}(\mathbf{x}) = (\mathbf{x}'\cdot\nabla)\mathbf{V},$$

where

$$\nabla\mathbf{V} = \partial_i V_j,$$

which has symmetric and antisymmetric parts described by

$$\partial_i V_j = \frac{1}{2}\epsilon_{ijk} W_k + S_{ij},$$

where S_{ij} is the shear tensor defined as $S_{ij} \equiv \frac{1}{2}(\partial_i V_j + \partial_j V_i)$ and $\mathbf{W} = \nabla \times \mathbf{V}$, the vorticity.

This integral may be simplified by noting that $\int \frac{1}{4\pi}|\mathbf{x}'|\,dx'^3$ is the inverse operator to $-2\nabla^4$, in the same way that $\int \frac{1}{4\pi}\frac{1}{|\mathbf{x}'|}\,dx'^3$ is the inverse Laplacian, ∇^2. This is similar to how the pressure correction was calculated in §3.2.

The Green's function for this operator is

$$\begin{aligned} G(\mathbf{x},\mathbf{x}') = & \ \tfrac{1}{4K^3} \ \left[e^{-K(\mathbf{x}-\mathbf{x}')} H(\mathbf{x}-\mathbf{x}') + e^{K(\mathbf{x}-\mathbf{x}')} H(\mathbf{x}'-\mathbf{x})\right], \\ + & \ \tfrac{1}{4K^2} \ \left[(\mathbf{x}-\mathbf{x}')e^{-K(\mathbf{x}-\mathbf{x}')} H(\mathbf{x}-\mathbf{x}') + (\mathbf{x}'-\mathbf{x})e^{K(\mathbf{x}-\mathbf{x}')} H(\mathbf{x}'-\mathbf{x})\right], \end{aligned}$$

where H is the Heaviside step function.

Thus,

$$\mathbf{b}(\Delta\varphi - \mathbf{a}\cdot\mathbf{V}) = -2\mathbf{b}(\mathbf{x}) \int \frac{dx'}{4\pi} G(x,x')\,(\partial_k j_i(\mathbf{x}-\mathbf{x}'))\,S_{ij}.$$

3.4 Angular Momentum Flux

The idea now is to compare the angular momentum flux to the magnetic helicity flux calculated in the last section. The angular momentum flux can simply be written down as

$$\mathcal{L} \equiv r\left[\rho\langle u_r u_\phi\rangle - \langle b_r b_\phi\rangle/4\pi\right],$$

and when cast into Cartesian coordinates is,

$$\mathcal{L} = \rho V_A^2 \left[\frac{\langle u_x u_y \rangle}{V_A^2} - \frac{\langle b_x b_y \rangle}{4\pi\rho V_A^2} \right],$$

where

$$\langle v_x v_y \rangle \equiv \mathrm{Re} \left[\int dx \, (v_x^* v_y) \right],$$

and similarly,

$$\langle b_x b_y \rangle \equiv \mathrm{Re} \left[\int dx \, (b_x^* b_y) \right].$$

The latter of these equations is the Maxwell stress while the former is the fluid momentum or Reynolds stress.

Chapter 4

Results and Discussion

4.1 Initial Conditions

A linear perturbation in the radial magnetic field was evolved according to the linear equations of motion, (3.2a)-(3.2c). The perturbation is characterized by a Gaussian with height of 1.0 and a full width half maximum of 10.0. To ensure that $\nabla \cdot \mathbf{b} = 0$ is satisfied, a corresponding perturbation in the azimuthal component of the magnetic field and is equal to $-\frac{3}{2i\bar{\omega}_A}\partial_x \mathbf{b}_x$. These initial conditions are put more clearly in the following form:

$$\mathbf{b}_x(x,0) = e^{\frac{(x-64)^2}{2\sigma^2}} \tag{4.1a}$$

$$\mathbf{b}_y(x,0) = -\frac{3}{2i\bar{\omega}_A}\partial_x \mathbf{b}_x(x,0) \tag{4.1b}$$

$$\mathbf{b}_z(x,0) = 0 \tag{4.1c}$$

$$\mathbf{u} = 0 \tag{4.1d}$$

These initial conditions were chosen in such a way as to create a linear perturbation in the magnetic field.

It is also important to specify the behaviour of the solution on the boundaries. The solution is calculated over a region from x=0 to x=128 with the radial perturbation centred at x=64. The requirement is that the solution go smoothly to zero on the edges, this will also be enforced for the solution of Q in the pressure correction step.

A graphical representation of the initial conditions is given in figures 4.1.

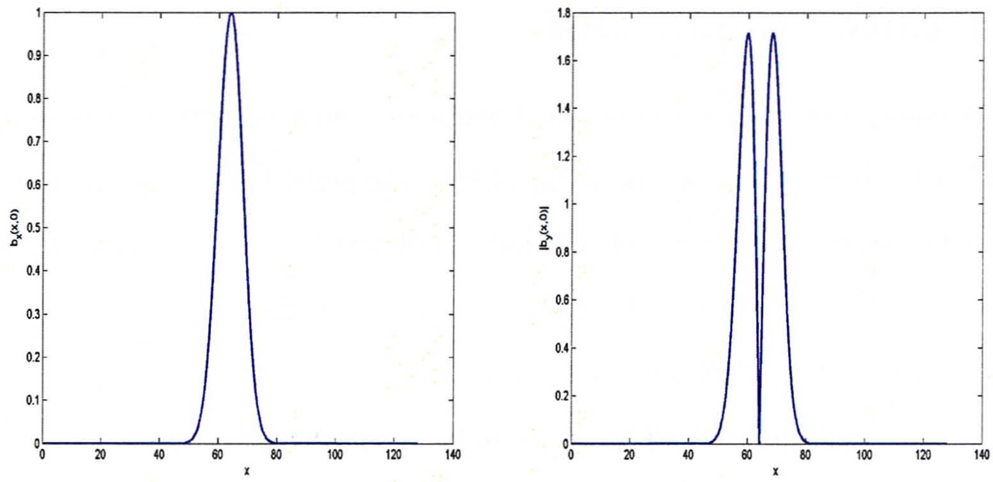

Figure 4.1: Initial conditions. Plotted are the amplitudes of the radial and azimuthal magnetic fields as a function of position at t=0.

Equations (3.1a)-(3.1c) are characterized by the normalized parameters κ and $\bar{\omega}_A$. The parameters κ and $\bar{\omega}_A$ were taken at discrete values of $3 \cdot 2^{-1}$, 2^0 , $3 \cdot 2^{-2}$, 2^{-1}, $3 \cdot 2^{-3}$, 2^{-2}, 2^{-3}, $3 \cdot 2^{-4}$

4.2 Test Cases

The first test case will be a test of the growth rate of the radial mode when $\kappa \ll \bar{\omega}_A \ll 1$. With these parameters the dispersion relation predicts a growth rate of $\sqrt{3}k_\phi V_A$ which when put into the dimensionless units used in the numerical code is $\sqrt{3}$. The results of this test can be seen in figure 4.2.

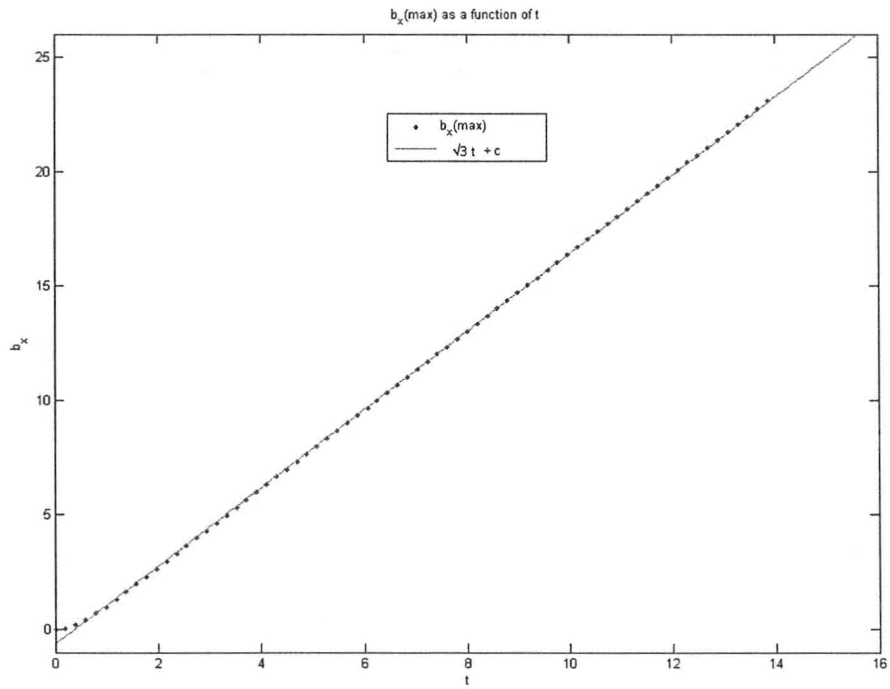

Figure 4.2: The growth rate of the radial mode with a Gaussian perturbation in the radial magnetic field and a corresponding perturbation in the y-component of the field is predicted to be $\sqrt{3}$. Plotted above is the natural logarithm of the maximum amplitude of the radial mode as a function of time. Along with the solution from the code is a line with a slope of $\sqrt{3}$. The above calculation is a robust result and is consistent with a calculation done with no pressure term in equation (3.2b) as well as the condition that $\kappa \ll \bar{\omega}_A \ll 1$.

A result using the MRI dispersion relation from Balbus & Hawley (1991) is that a perturbation will grow for k_z/k_ϕ e-foldings in the asymptotic limit ($\kappa \ll \bar{\omega}_A \ll 1$). With the Cartesian coordinates used this prediction becomes $\frac{k_z}{k_y} = \frac{1}{\kappa}$. A test of this case is given in 4.3.

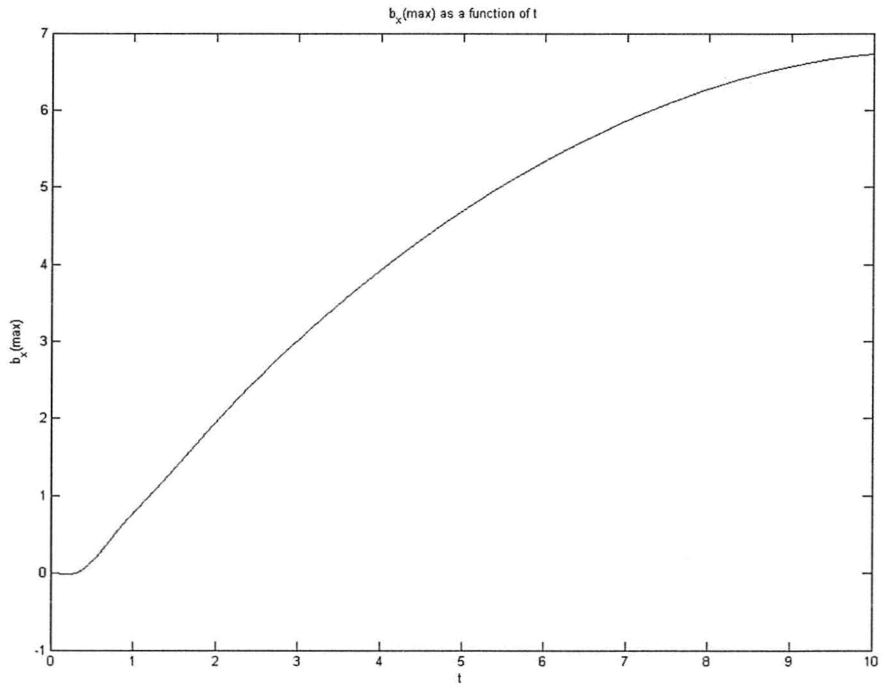

Figure 4.3: The amplitude of the radial mode grows exponentially for approximately 7 e-foldings. The growth rate of the radial mode with a Gaussian perturbation in the radial magnetic field and a corresponding perturbation in the y-component of the field is expected to grow for $\sim \frac{k_z}{k_\phi}$ e-folding times. The parameters in the above plot are $\kappa = \bar{\omega}_A = 2^{-3}$ so that the number of e-foldings expected is ~ 8 which is in rough agreement with the above plot.

4.3 Magnetic and Velocity Fields

In this section I present the time evolution of the magnetic and velocity fields. The radial magnetic field will be followed as well as the magnitude of the total magnetic field. The former can tell us about how each mode is evolving over time while the latter can tell us if the overall mode is growing or not. The plots of the modes which do not show growth and are thus uninteresting can be found in the Appendix.

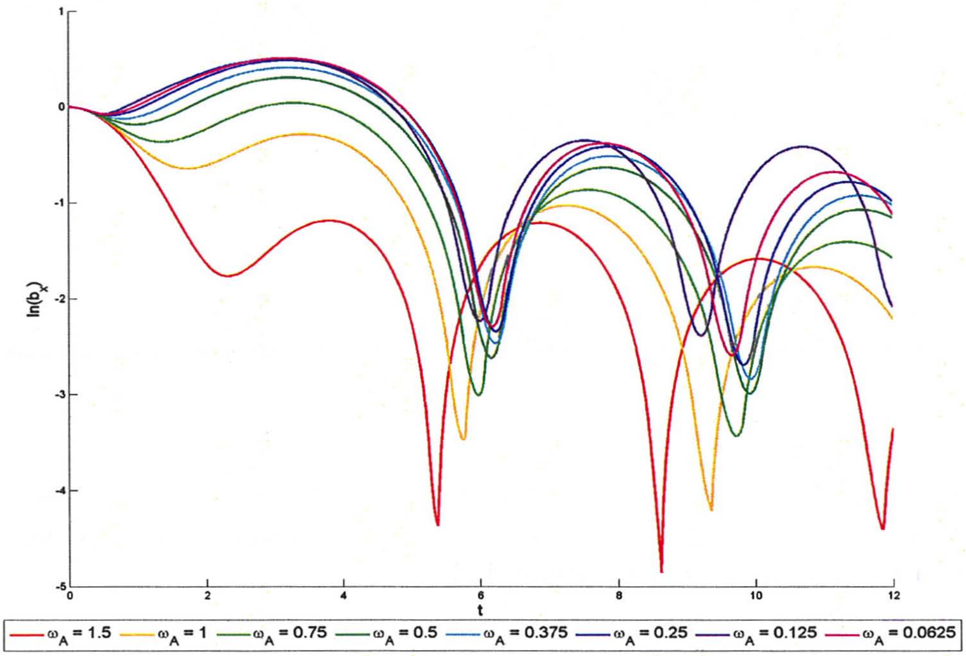

Figure 4.4: Varying $\bar{\omega}_A$ with $\kappa = 0.5$. Modes with values of $\bar{\omega}_A$ between 0.5 and 0.0625 grow exponentially until $t \sim 3$ and then begin to oscillate temporally.

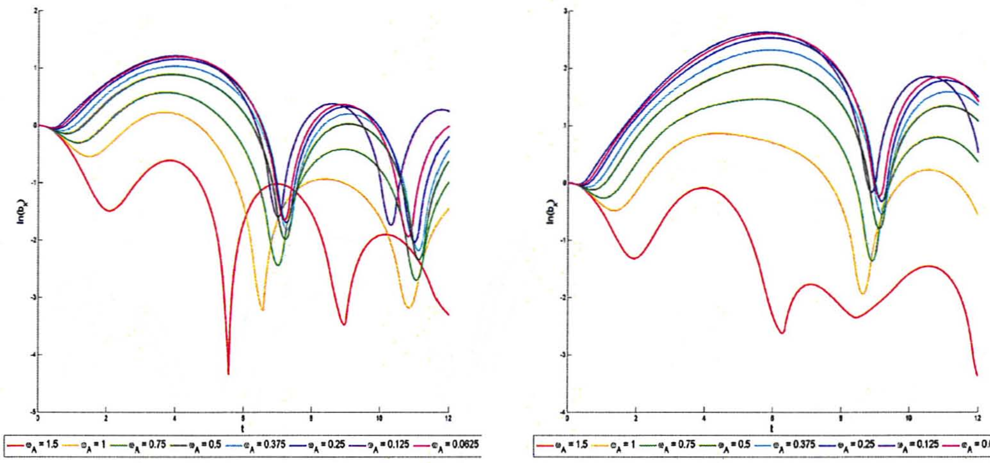

Figure 4.5: $\kappa = 0.375$ on the left, $\kappa = 0.25$ on the right. As κ is decreased, the exponentially growing phase is increased in duration. As $\bar{\omega}_A$ is decreased the modes approach an asymptotic limit.

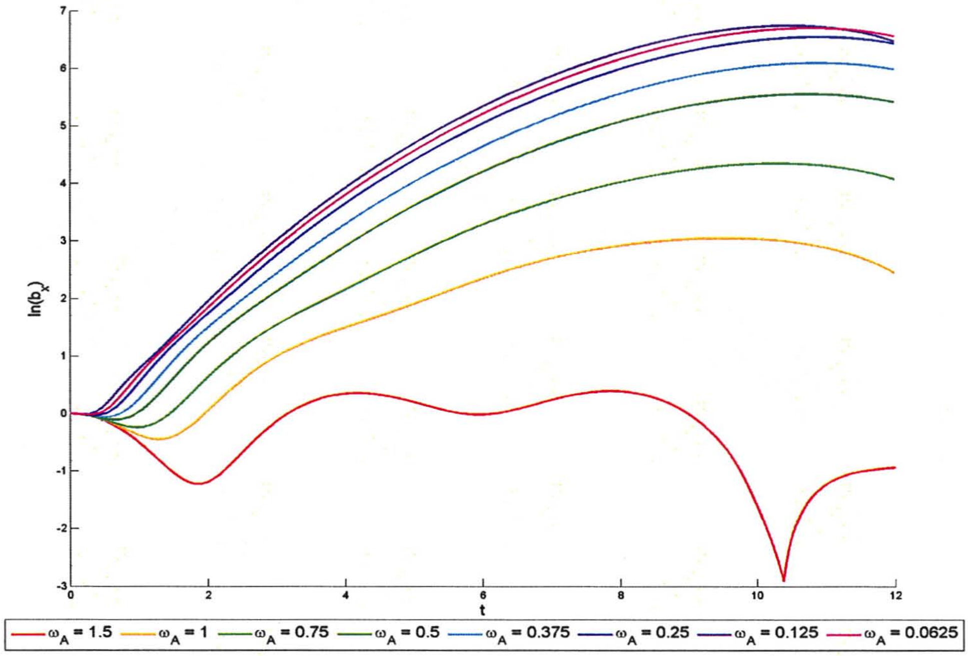

Figure 4.6: Radial magnetic mode with $\kappa = 0.125$. A long lived growing mode is present which corresponds to the asymptotic limit when $\bar{\omega}_A \ll 1$ for small κ.

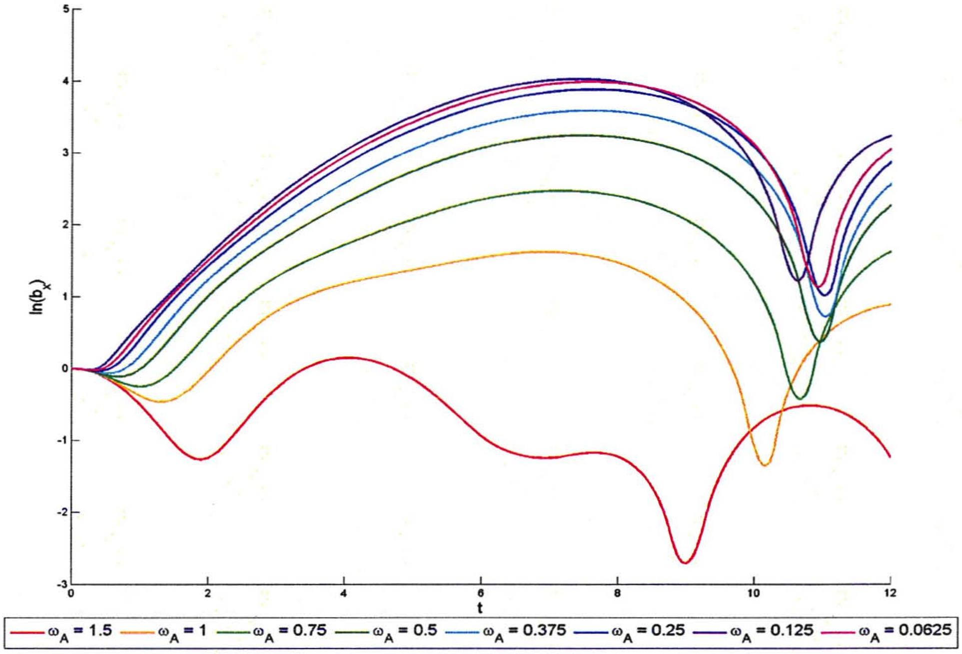

Figure 4.7: Radial magnetic mode with $\kappa = 0.0625$

The plots of the hydrodynamic modes are similar to the magnetic modes and simply show the relation to the magnetic modes.

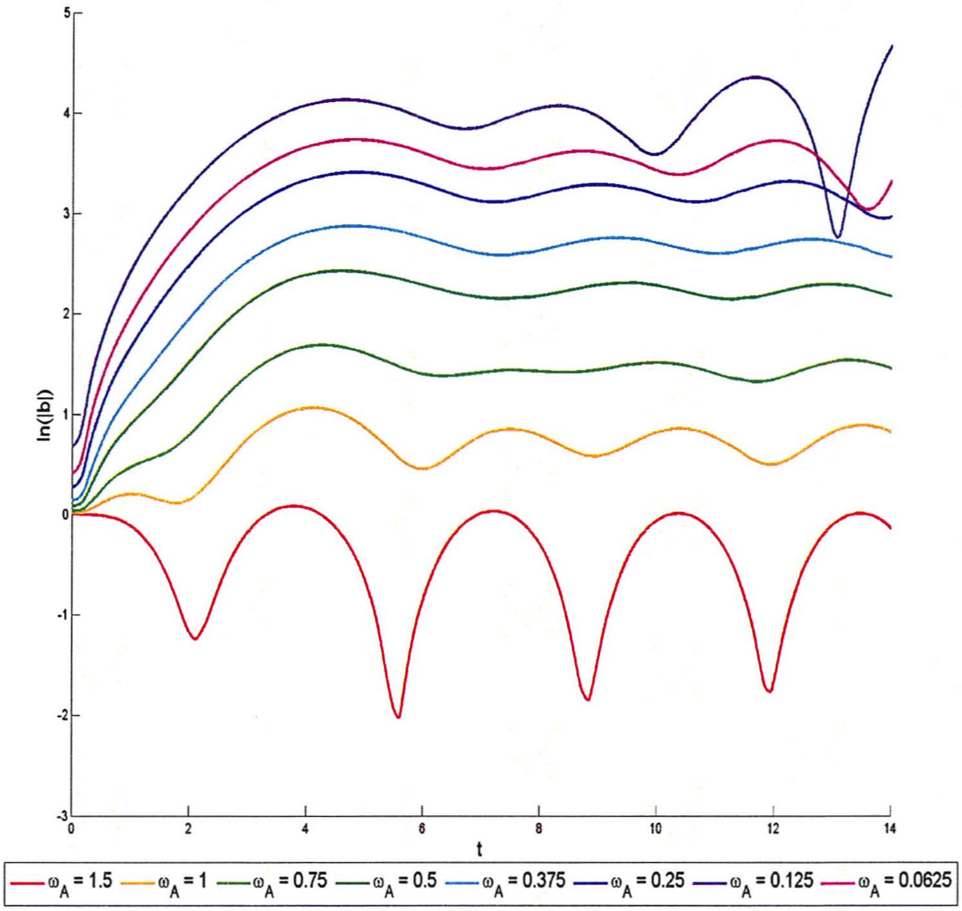

Figure 4.8: Total magnetic mode with $\kappa = 0.375$.

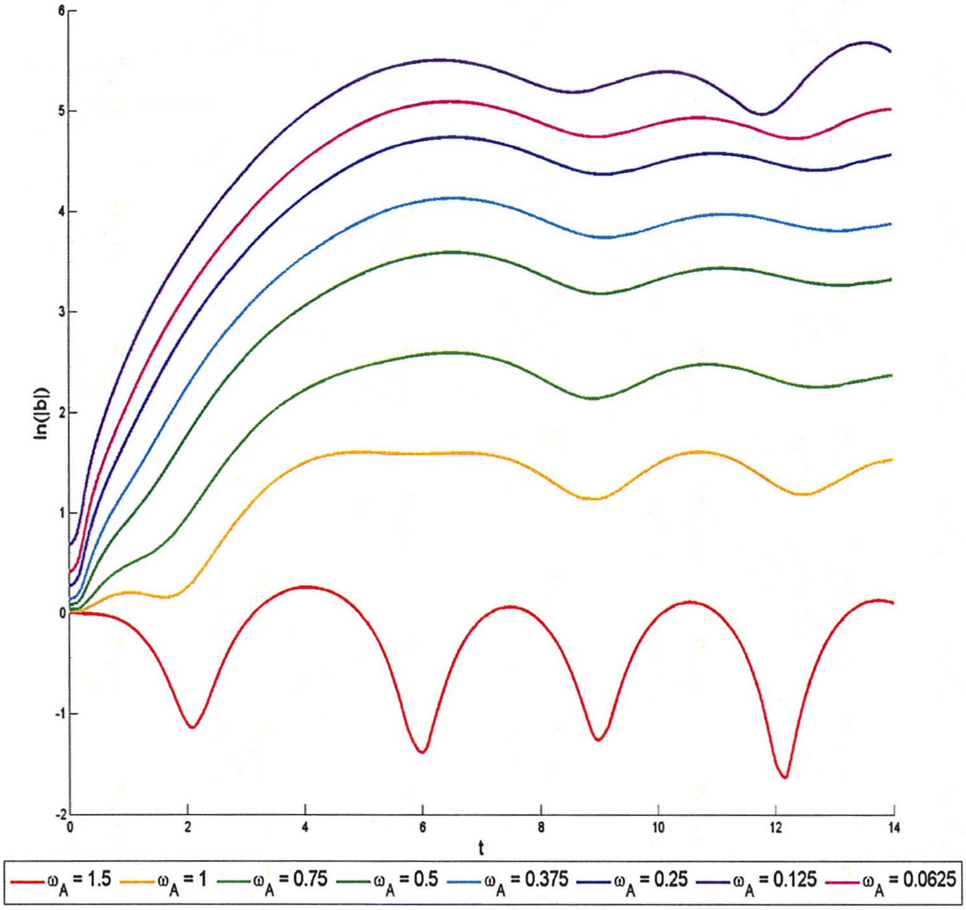

Figure 4.9: Total magnetic mode with $\kappa = 0.25$.

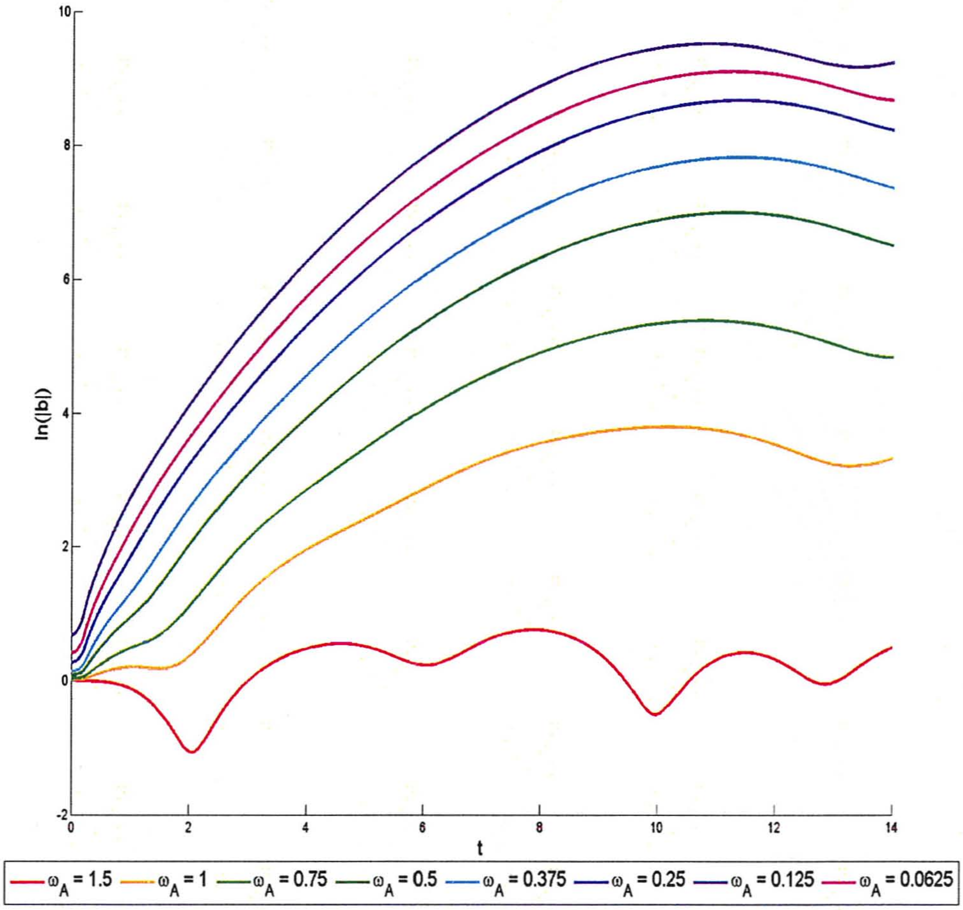

Figure 4.10: Total magnetic mode with $\kappa = 0.125$.

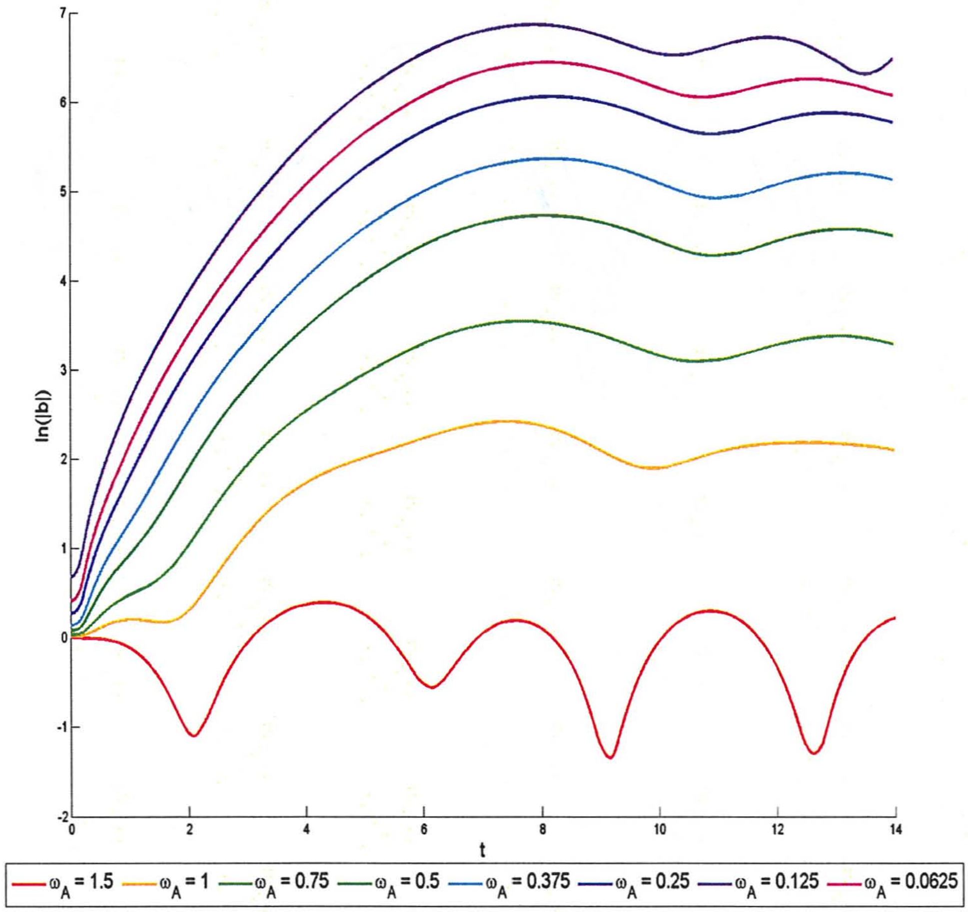

Figure 4.11: Total magnetic mode with $\kappa = 0.0625$.

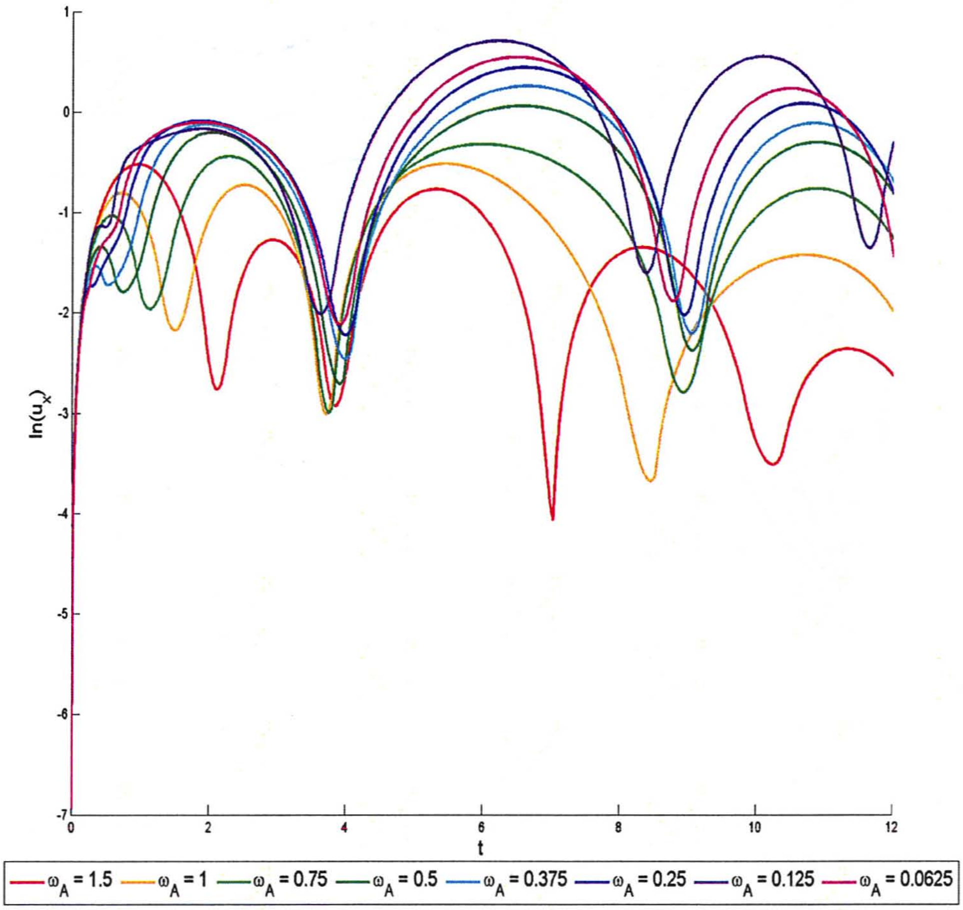

Figure 4.12: Radial hydrodynamic mode for $\kappa = 0.375$.

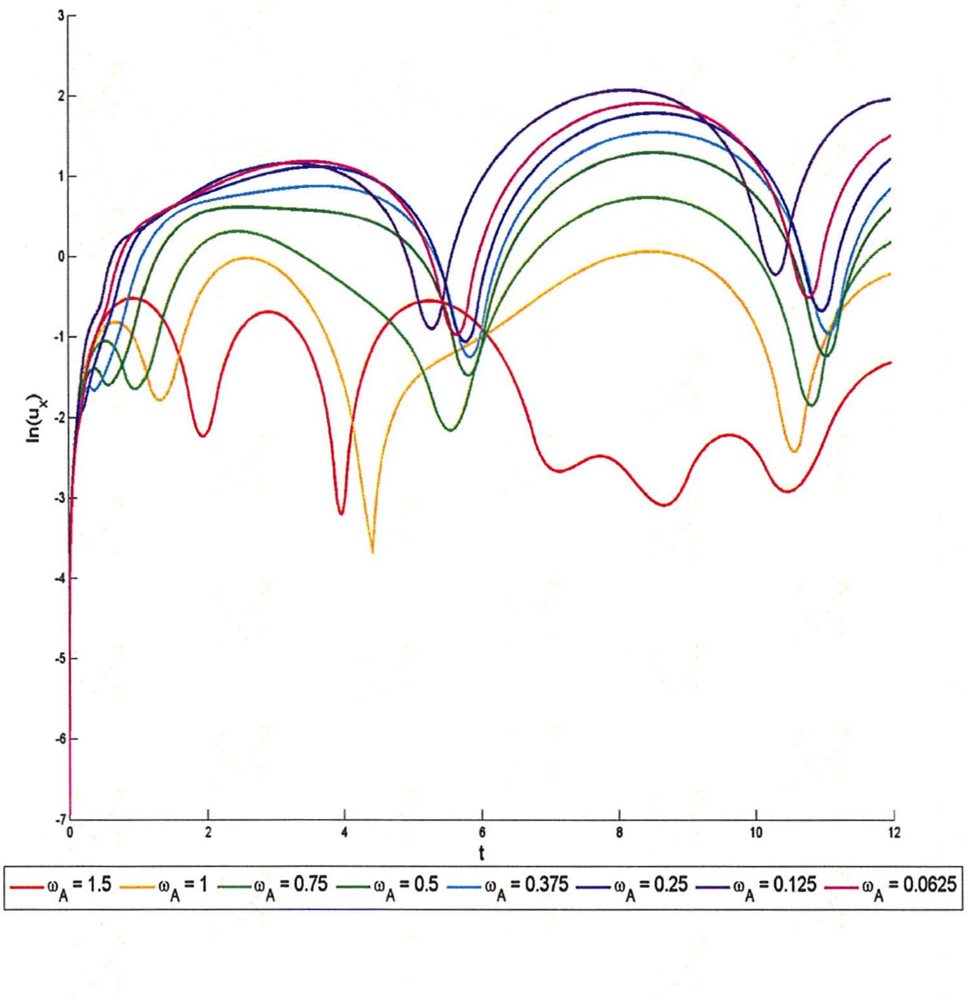

Figure 4.13: Radial hydrodynamic mode for $\kappa = 0.25$.

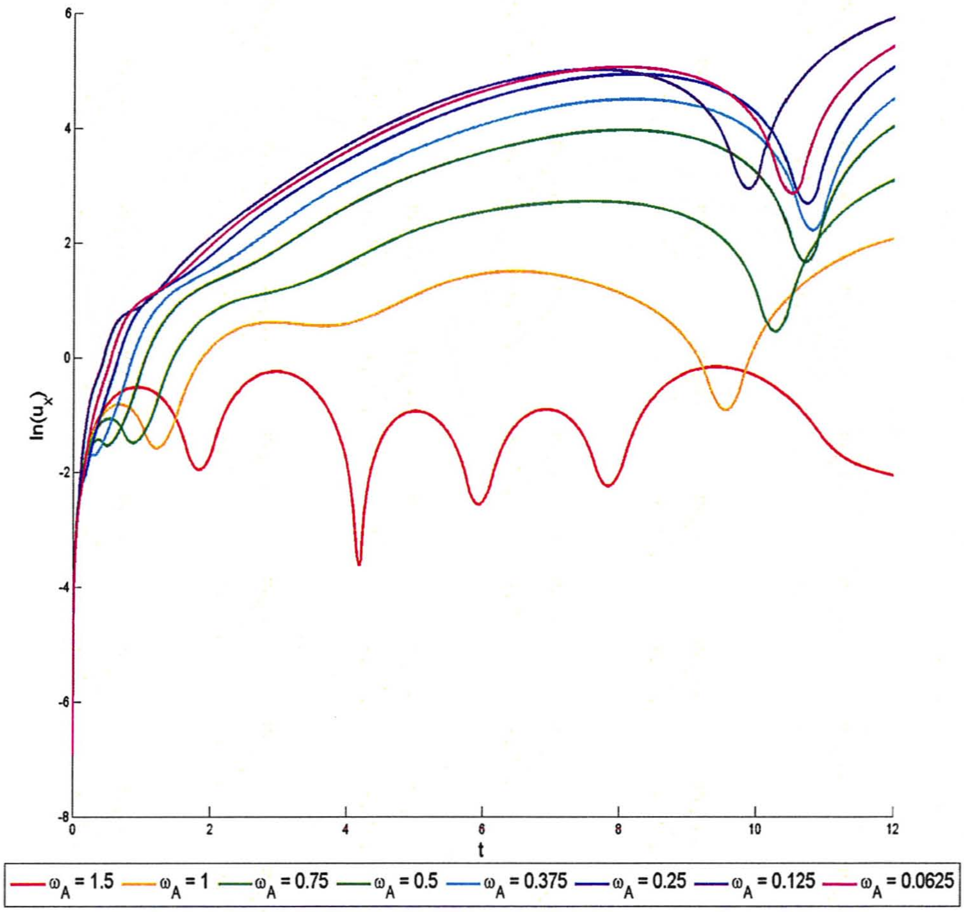

Figure 4.14: Radial hydrodynamic mode for $\kappa = 0.125$.

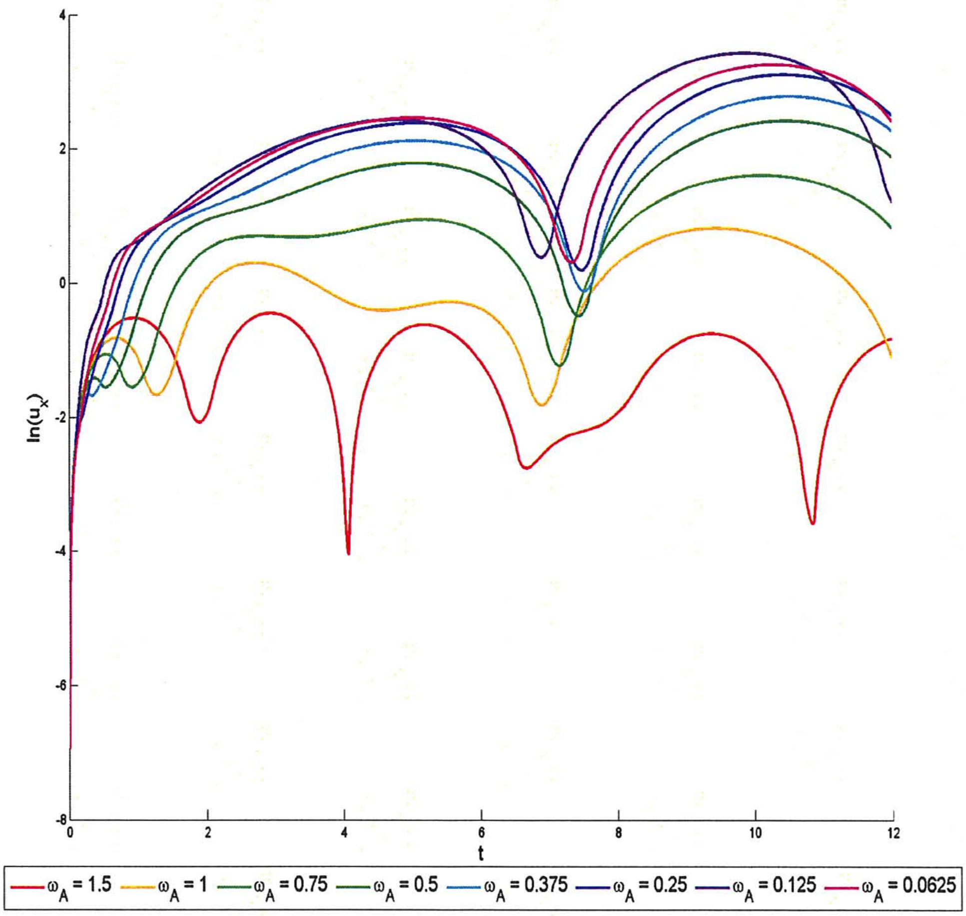

Figure 4.15: Radial hydrodynamic mode for $\kappa = 0.0625$.

4.4 Quadratic Quantities

The following plots are of the magnetic helicity flux along the z-direction as a function of time.

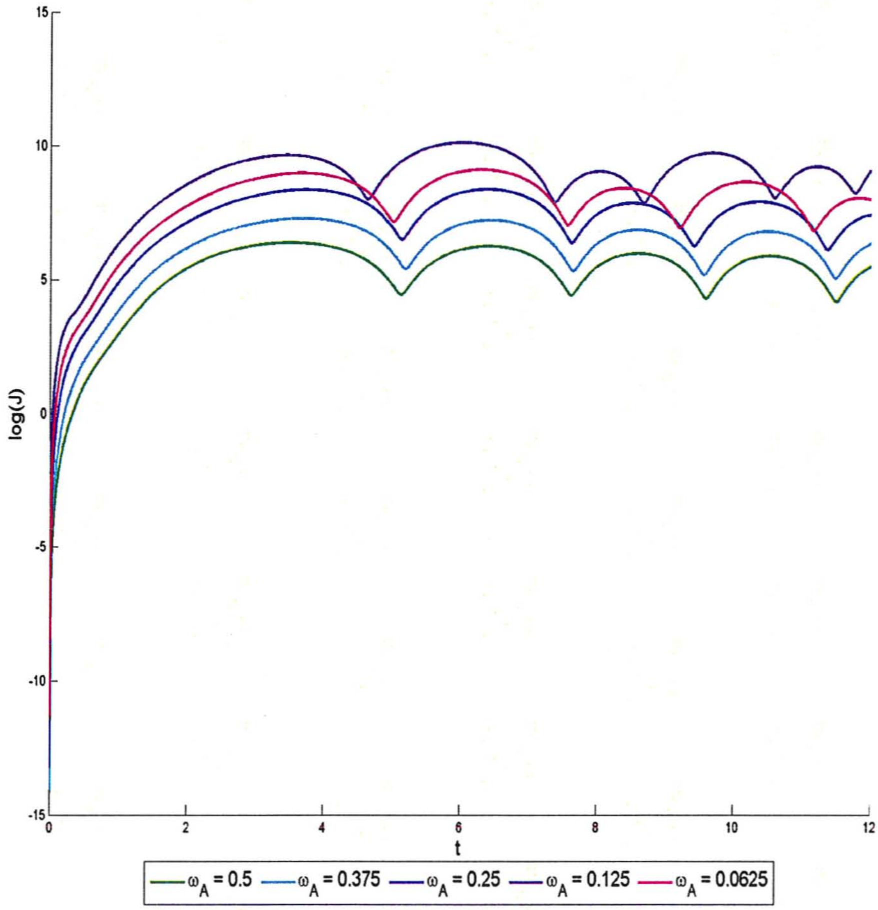

Figure 4.16: Mean magnetic helicity flux with $\kappa = 0.375$.

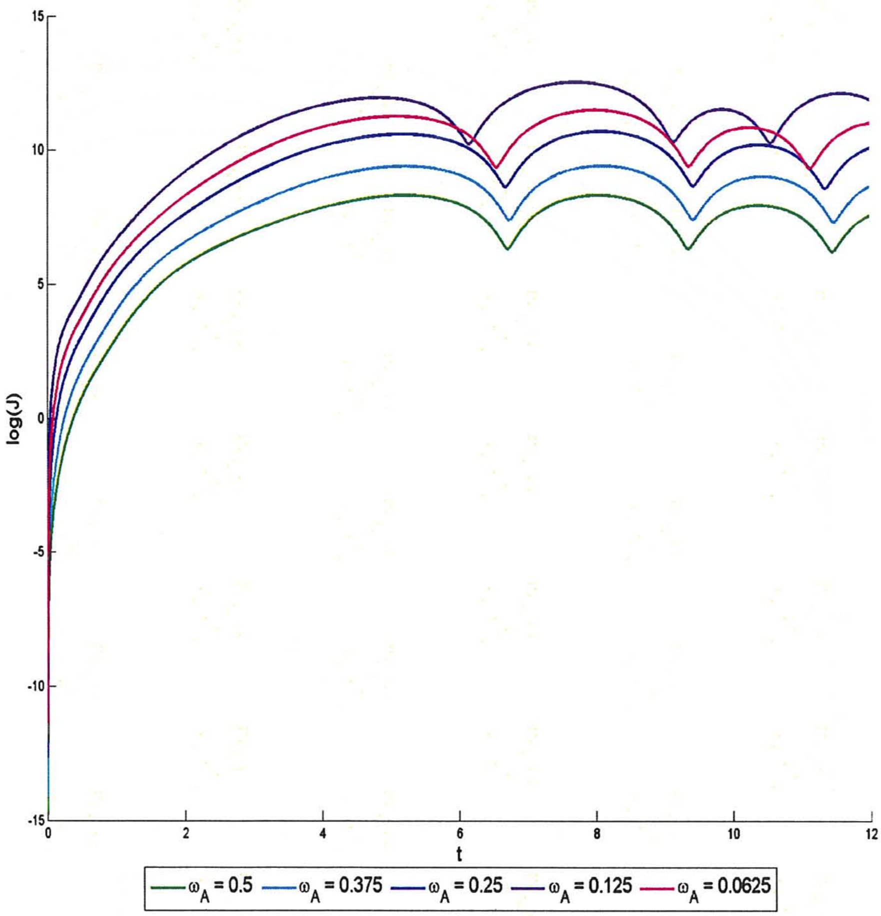

Figure 4.17: Mean magnetic helicity flux with $\kappa = 0.25$.

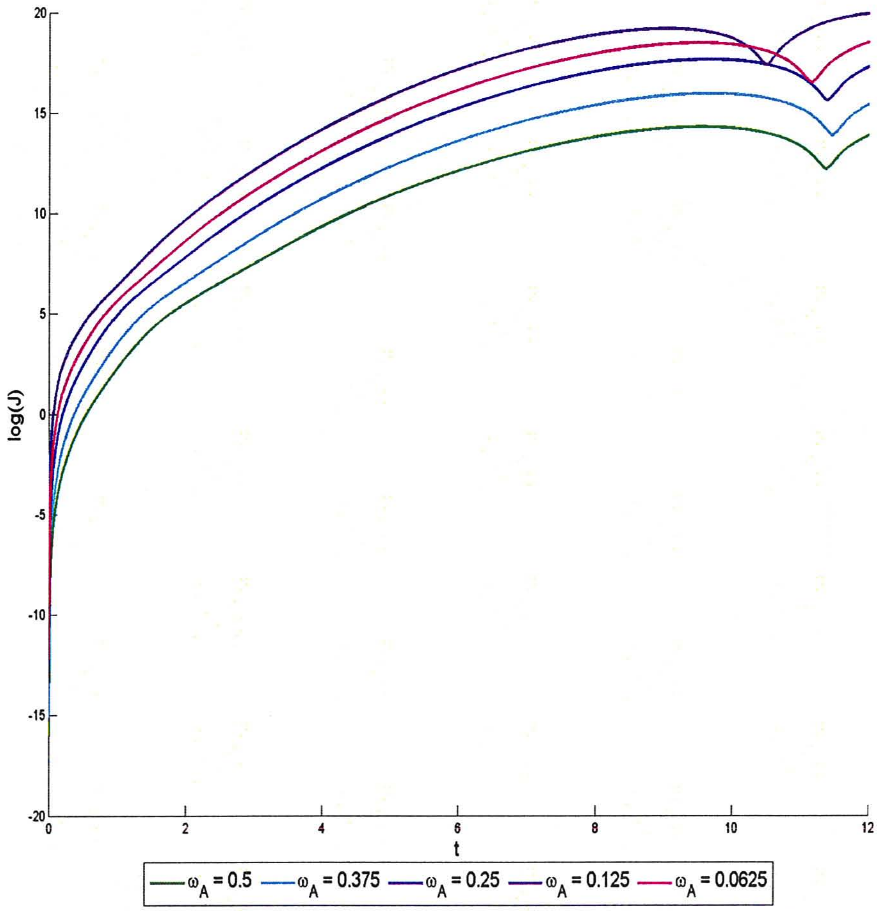

Figure 4.18: Mean magnetic helicity flux with $\kappa = 0.125$.

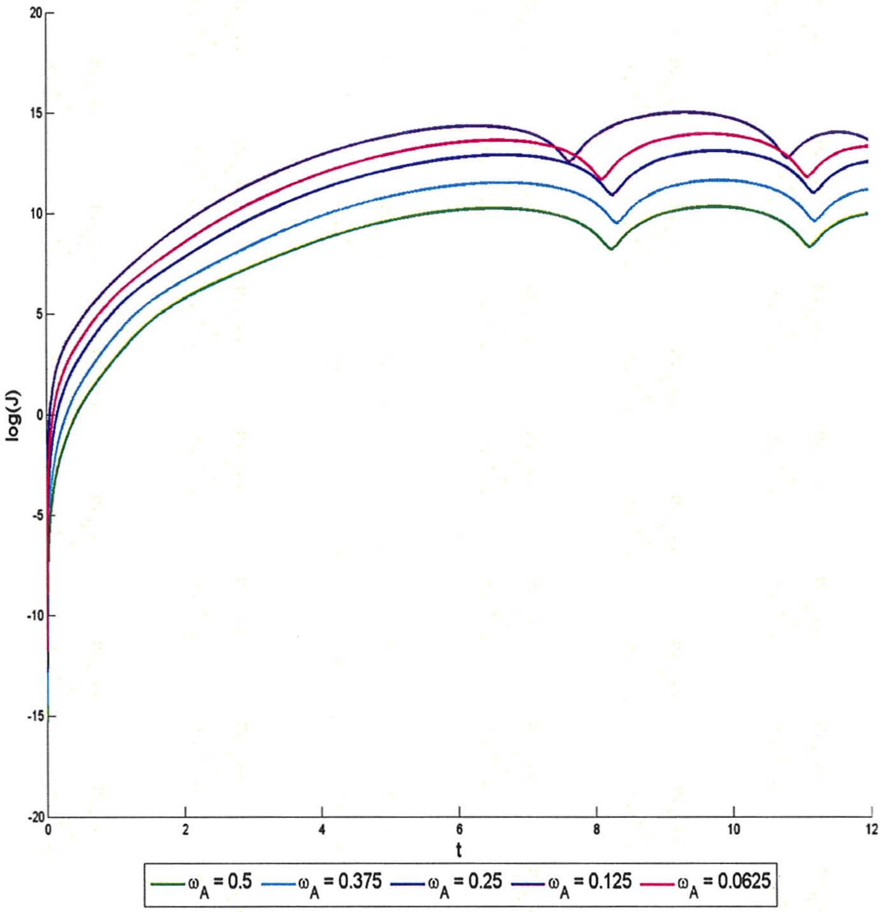

Figure 4.19: Mean magnetic helicity flux with $\kappa = 0.0625$.

The following plots are the mean angular momentum flux as a function of time defined in the same way as the magnetic helicity flux,

$$\mathcal{L} = \rho V_A^2 \left[\frac{\langle u_x u_y \rangle}{V_A^2} - \frac{\langle b_x b_y \rangle}{4\pi \rho V_A^2} \right]$$

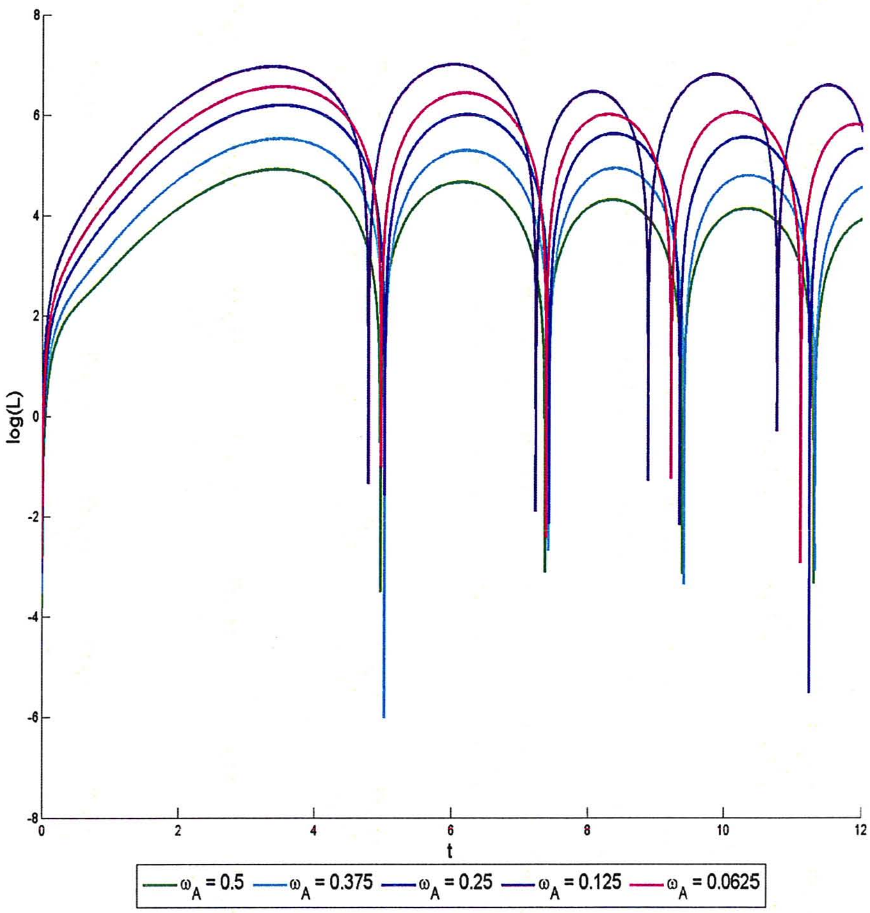

Figure 4.20: Mean of the angular momentum flux with $\kappa = 0.375$.

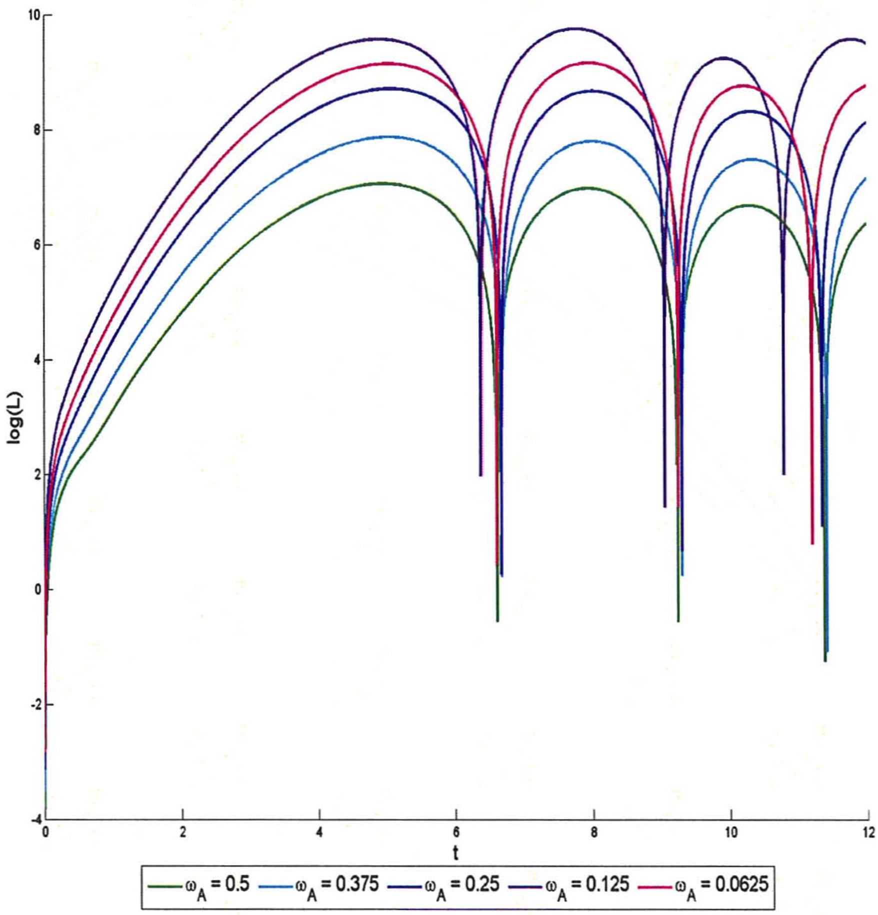

Figure 4.21: Mean of the angular momentum flux with $\kappa = 0.25$.

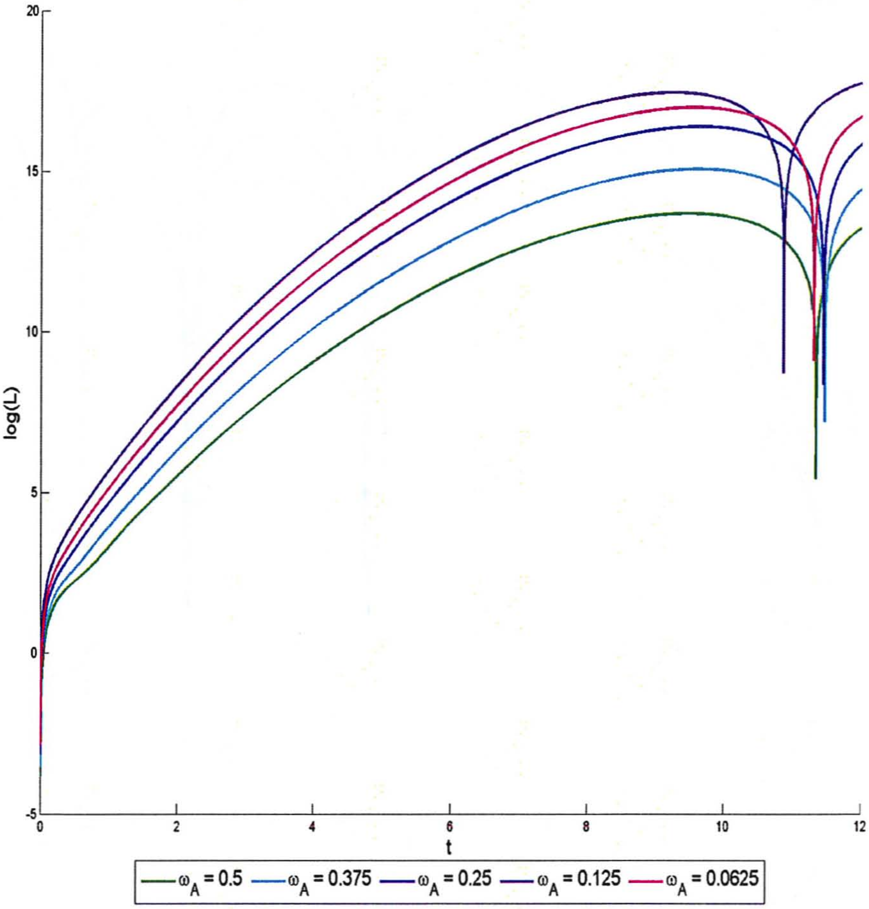

Figure 4.22: Mean of the angular momentum flux with $\kappa = 0.125$.

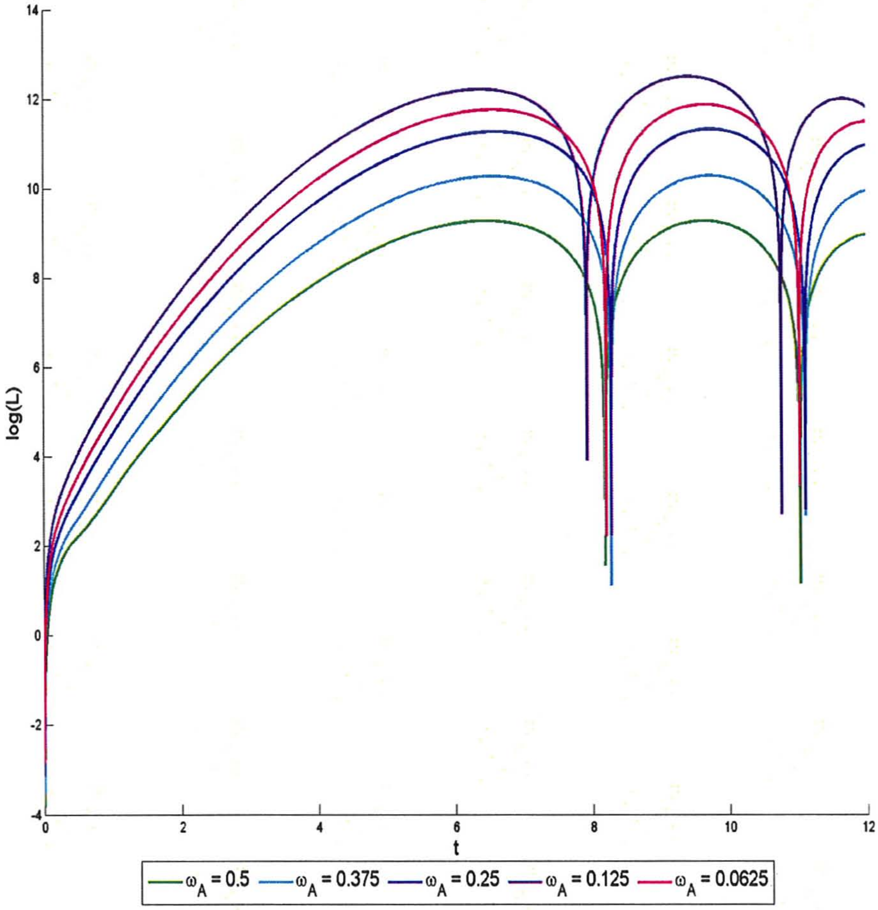

Figure 4.23: Mean of the angular momentum flux with $\kappa = 0.0625$.

Finally the ratio of the magnetic helicity flux to the angular momentum flux as a function of time. This ratio is approximately constant during the growing phase of the perturbations and is characterized by oscillations in time after this growing phase.

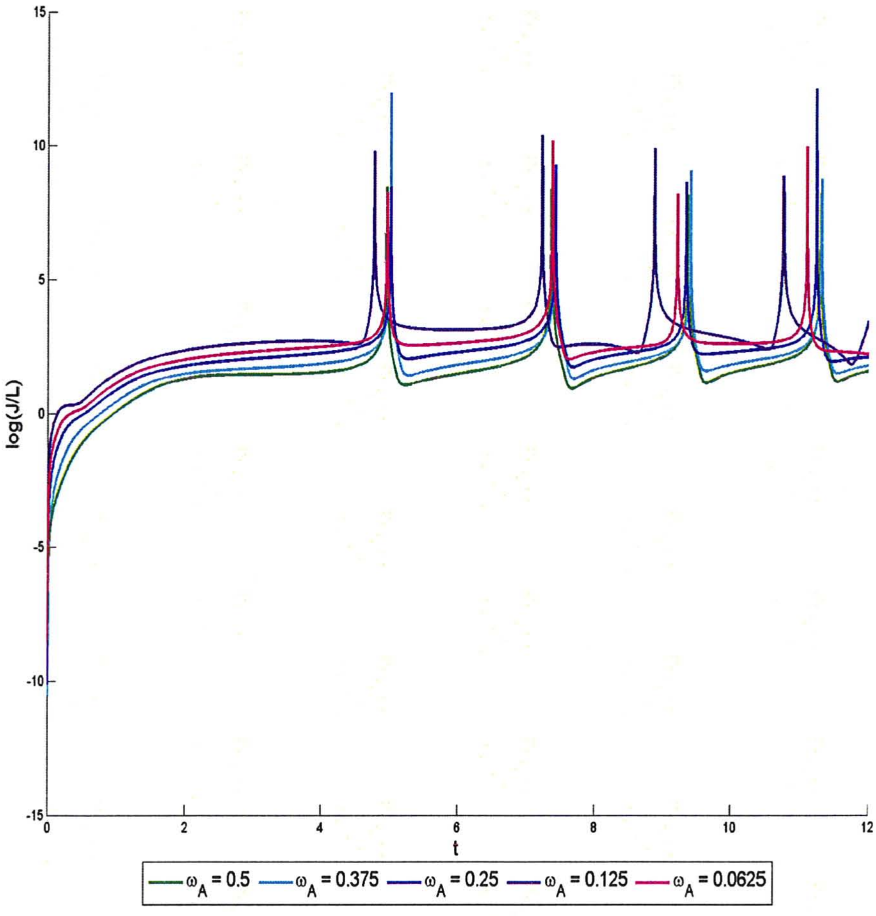

Figure 4.24: Ratio of the magnetic helicity flux to the angular momentum flux for $\kappa = 0.375$

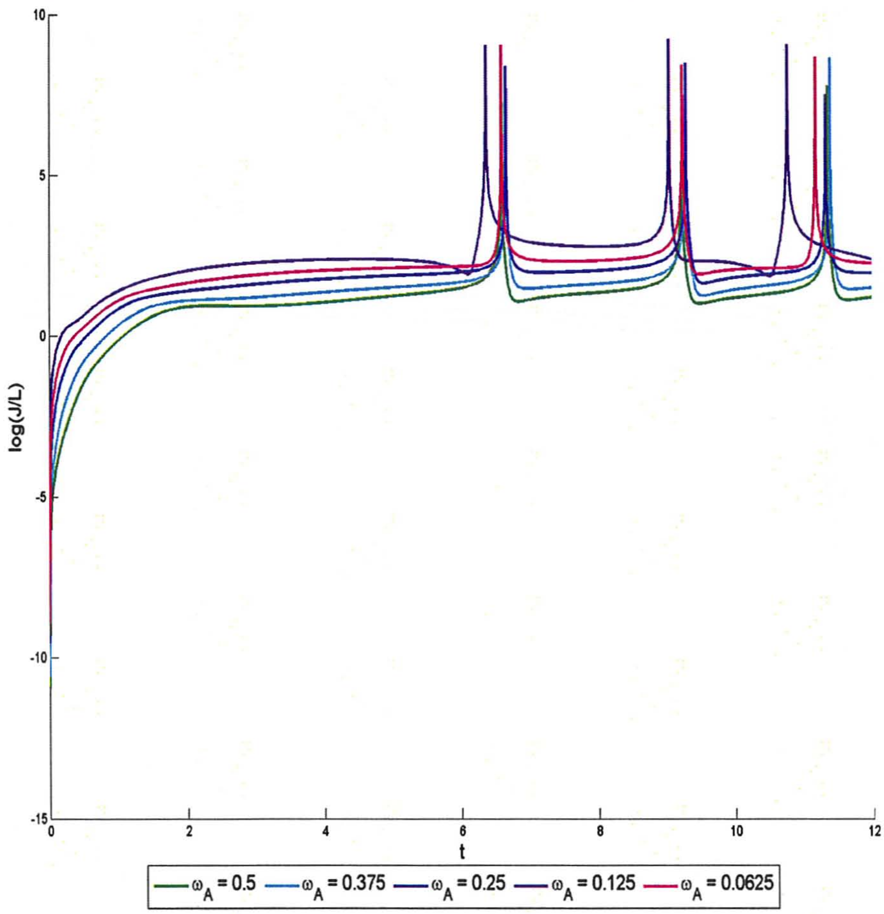

Figure 4.25: Ratio of the magnetic helicity flux to the angular momentum flux for $\kappa = 0.25$

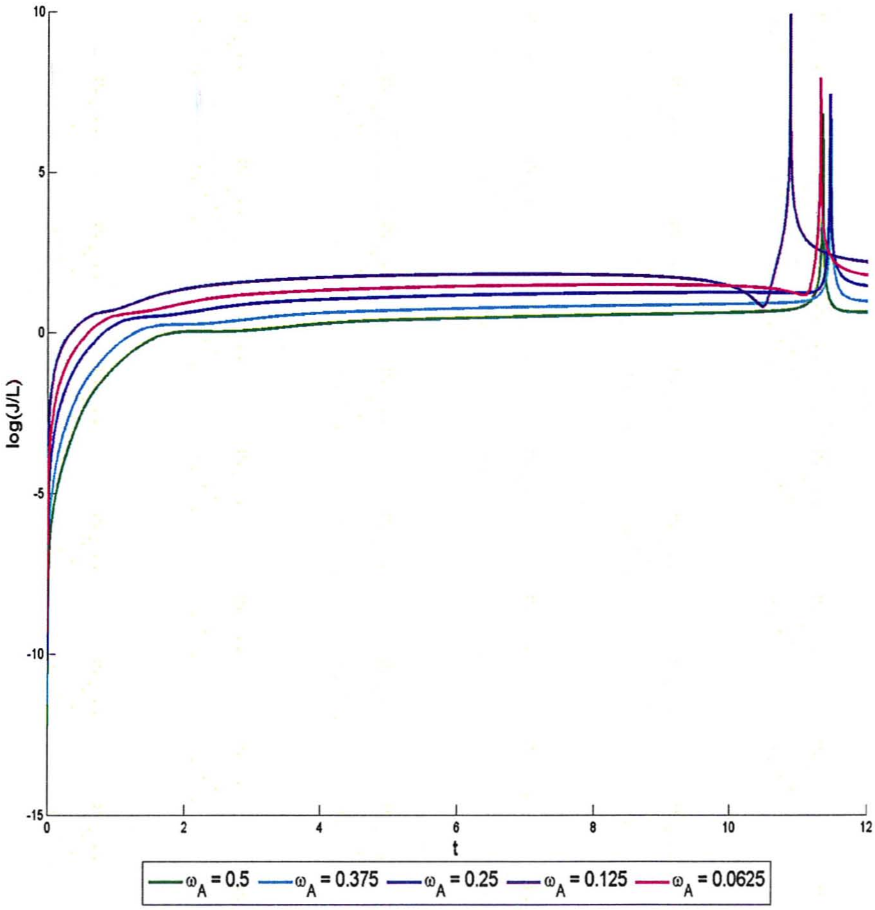

Figure 4.26: Ratio of the magnetic helicity flux to the angular momentum flux with $\kappa = 0.125$. The ratio is constant over the growing part of the solution.

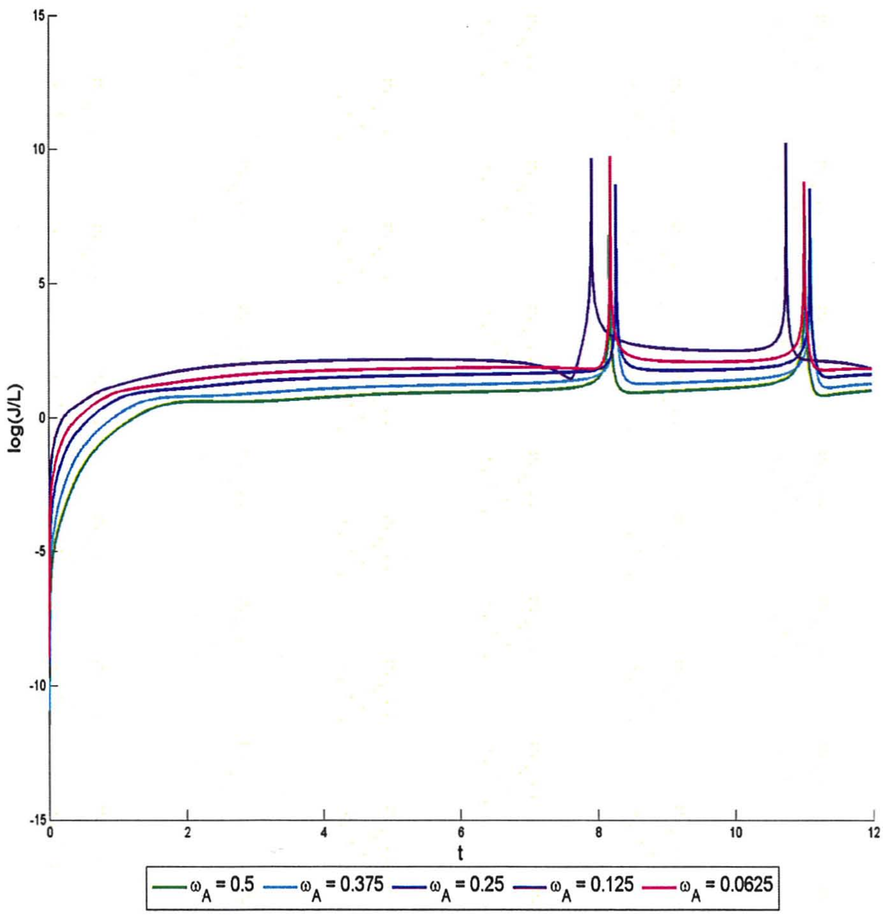

Figure 4.27: Ratio of the magnetic helicity flux to the angular momentum flux for $\kappa = 0.0625$

4.5 Discussion

The rate of growth for the magnetic and hydrodynamic modes are in agreement with the predictions for the MRI in the asymptotic limit. Specifically, the rate of growth in this limit should be $\sqrt{3}$ using the normalized variables, this is shown in figure 4.2. In addition, the time for which these modes grow is also in agreement in that a particular mode should grow for $\frac{1}{\kappa}$ e-folding times.

Growing modes were seen to occur when $\bar{\omega}_A$ was below 0.5 and κ was similarly small. In this regime, the mean of the magnetic helicity flux over time was found to grow and peak at a time corresponding to the peak of the magnetic and hydrodynamic modes. The angular momentum flux followed a similar pattern except that the growth rate was much lower than the magnetic helicity flux.

The ratio of the magnetic helicity flux to the angular momentum flux ought to be a constant over time by use of a simple argument. This argument is as follows: If the magnetic and hydrodynamic modes grow at the same rate, then any quadratic quantities in the perturbation variables should grow at the same rate as well. Checking figure 4.28, the individual modes do indeed grow at the same rate.

Checking figure 4.26, it is confirmed that the ratio of the magnetic helicity flux and the angular momentum flux are approximately constant over the times when the modes are exponentially growing. This suggests that the efficiency of these processes is approximately equal.

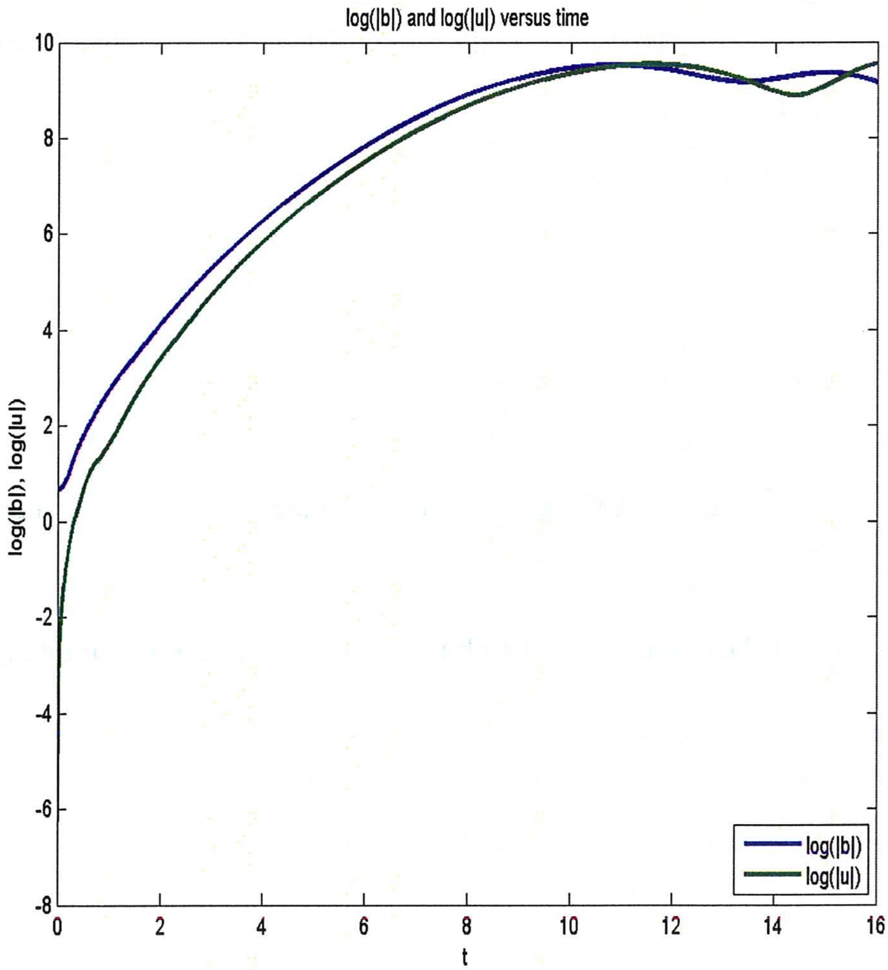

Figure 4.28: Magnitude of **b** and the magnitude of **u** as a function of time. The solutions to the equations of motion are characterized by exponentially growing solutions. These solutions show that the hydrodynamic and magnetic modes should have the same approximate growth rate.

Chapter 5

Conclusions

The intent of this thesis was to look at the ability of an accretion disk to both power a dynamo and accrete matter. The efficiency of these processes are captured in the magnetic helicicy and the angular momentum transports. The results of the simulations seem to show that the efficiency of the magnetic helicity transport is similar to the transport of angular momentum when the MRI in the accretion disk is in the asymptotic regime when the MRI is undergoing a growing mode.

The MRI was simulated in a locally Cartesian patch which the equations of motion were solved with a parameter space covering the asymptotic regime, that is when $\bar{\omega}_A \ll 1$ for small κ. The subsequent growth rate of the magnetic and hydrodynamic modes were consistent with predictions from the MRI dispersion relation for an azimuthal magnetic field laid out by Vishniac & Diamond (1992). A projection method, similar to how the incompressible Navier-Stokes equations are solved, was used to correct the pressure. To evolve the equations, a second order Runge-Kutta method was used.

The magnetic helicity flux was calculated using the definitions in Vishniac & Cho (2001), but with three additional terms due to the large scale background velocity field. This quantity is then integrated along x at each timestep with the intention of comparing it to the angular momentum flux. The angular momentum flux is the combination of the fluid momentum and the Maxwell stress due to the magnetic field and is similarly integrated along x to get a mean value of the flux. These quantities are important to describe both how the accretion disk transports its angular momentum and thus accretes matter as well as how the dynamo process in the disk works. The latter process is dependant on the generation of magnetic helicity on eddy scales and the transporting of this quantitiy to the large scale where the dynamo is powered. The flux of this quantitiy provides a term in the electromotive force which is parallel to the large scale magnetic field to complete the regenerative cycle necessary for the dynamo process.

The results of this calculation show that the efficiency at which the magnetic helicity is transported, is very similar to the efficiency at which the angular momentum is transported during the growing phase of a linear perturbation. This result follows from the simple argument that the magnetic and hydrodynamic perturbations grow at the same rate, then the quadratic quantities derived from them ought to be growing at the same rate as well.

The various growing modes all display an oscillating behaviour with the direction of the transport of the quadratic quantities changing after the modes finish growing oscillating after this point.

Appendix

5.1 Extra Plots

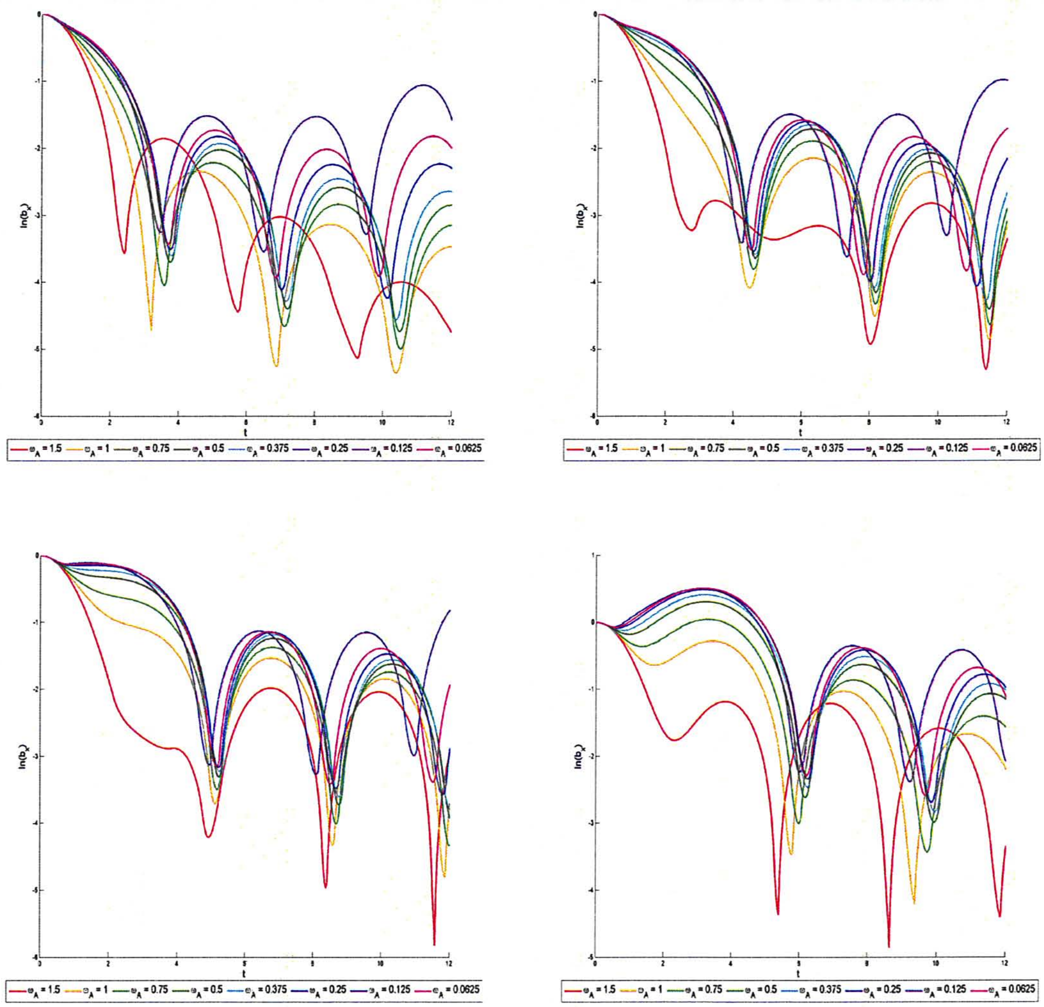

Figure 5.1: Radial mode of the magnetic field for $\kappa = 1.5$ (top left), $\kappa = 1.0$ (top right), $\kappa = 0.75$ (lower left), $\kappa = 0.5$ (lower left). Since the parameters lie outside of the asymptotic regime there is little to no growth in these modes.

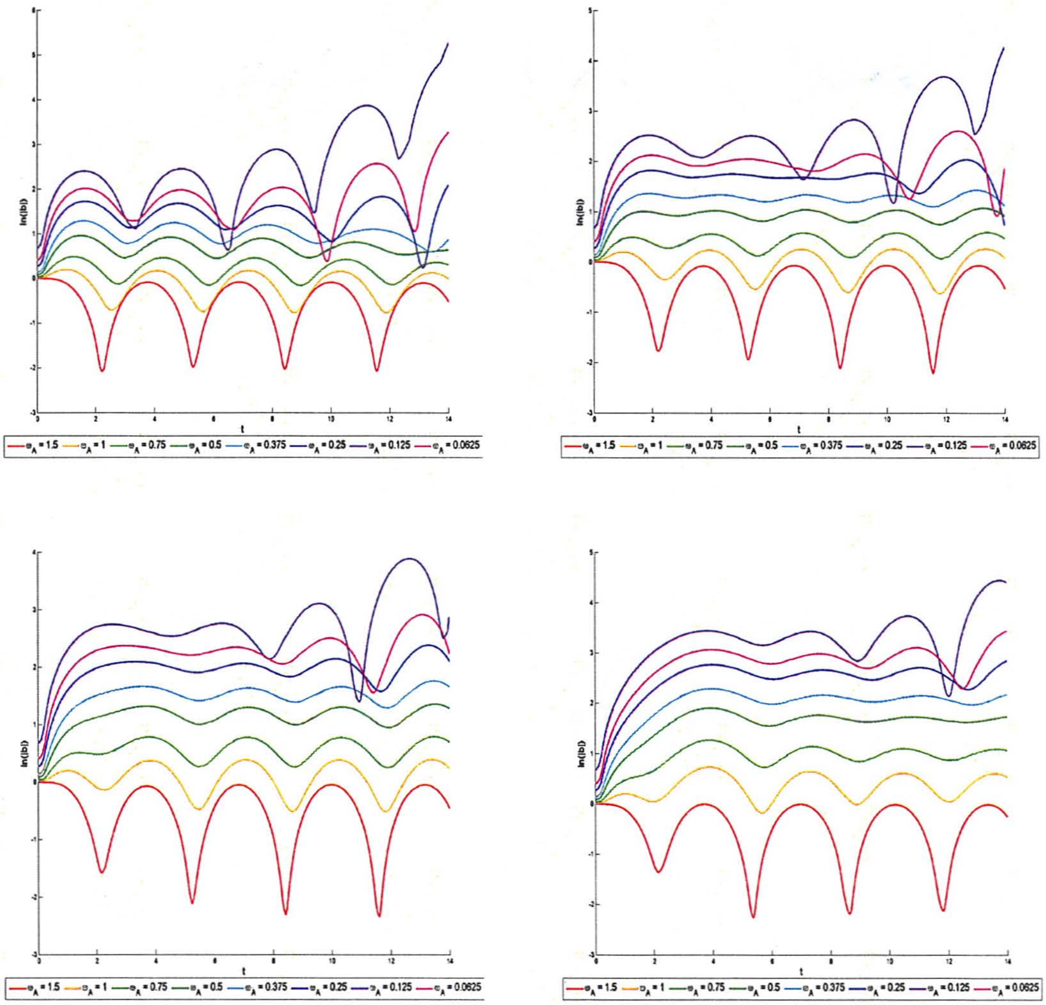

Figure 5.2: Magnitude of the magnetic mode for $\kappa = 1.5$ (top left), $\kappa = 1.0$ (top right), $\kappa = 0.75$ (lower left), $\kappa = 0.5$ (lower left). Since the parameters lie outside of the asymptotic regime there is little to no growth in these modes.

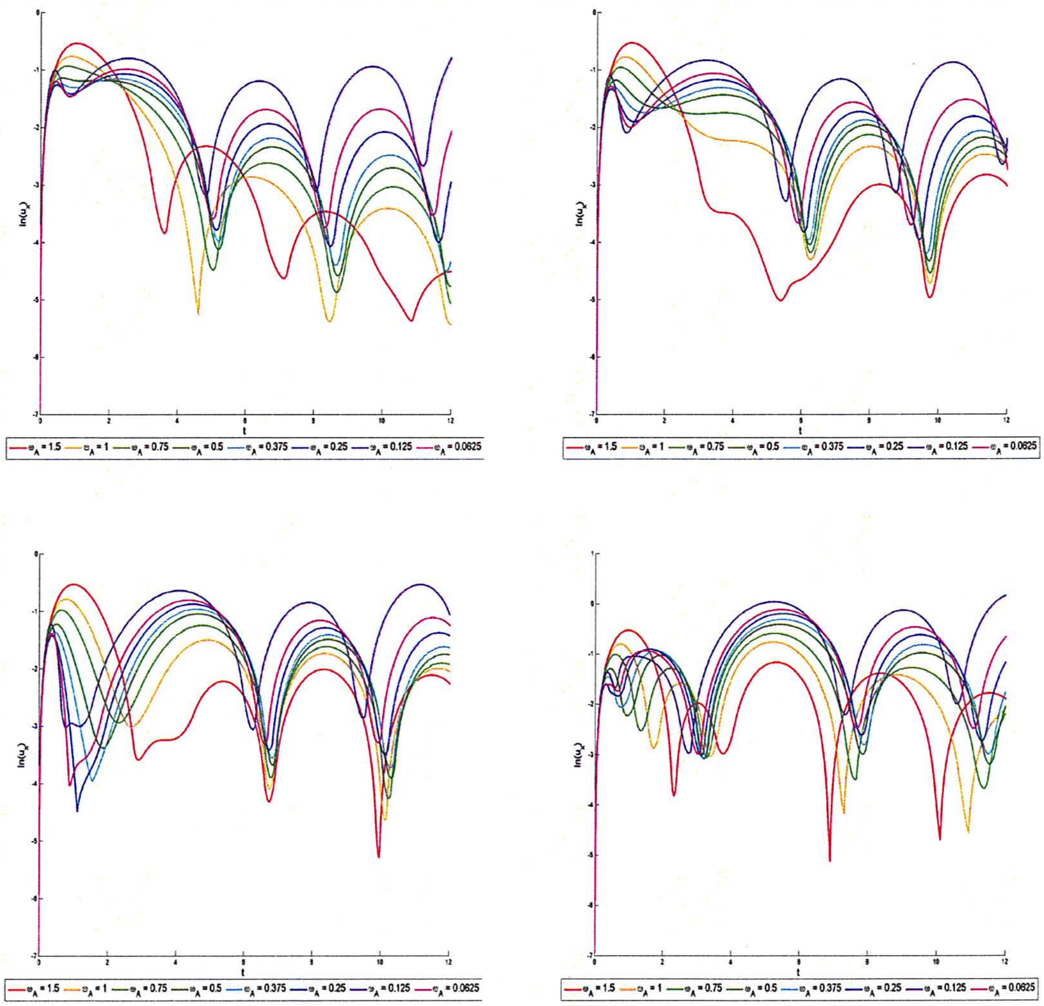

Figure 5.3: Radial mode of the velocity field for $\kappa = 1.5$ (top left), $\kappa = 1.0$ (top right), $\kappa = 0.75$ (lower left), $\kappa = 0.5$ (lower left). Since the parameters lie outside of the asymptotic regime there is little to no growth in these modes.

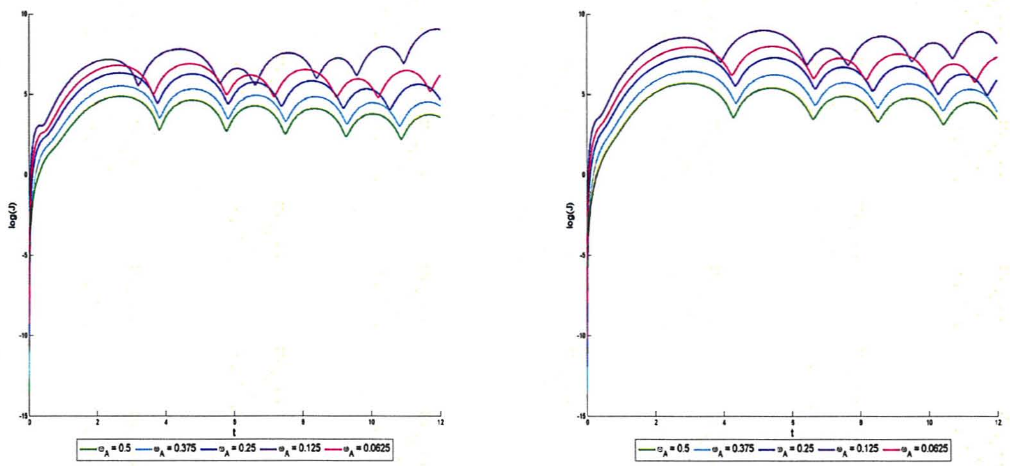

Figure 5.4: Mean of the magnetic helicity flux for $\kappa = 1.5$ (top left), $\kappa = 1.0$ (top right), $\kappa = 0.75$ (lower left), $\kappa = 0.5$ (lower left). Since the parameters lie outside of the asymptotic regime there is little to no growth in these modes.

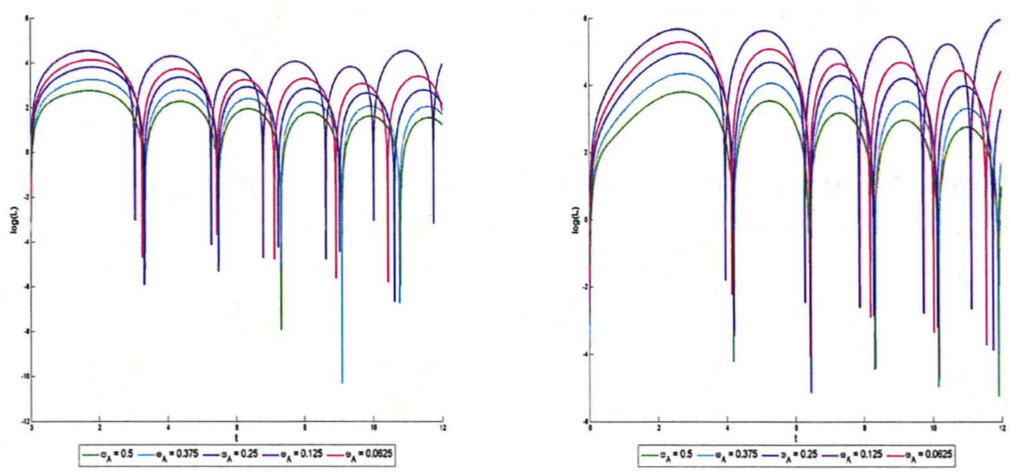

Figure 5.5: Mean of the angular momentum flux for $\kappa = 1.5$ (top left), $\kappa = 1.0$ (top right), $\kappa = 0.75$ (lower left), $\kappa = 0.5$ (lower left). Since the parameters lie outside of the asymptotic regime there is little to no growth in these modes.

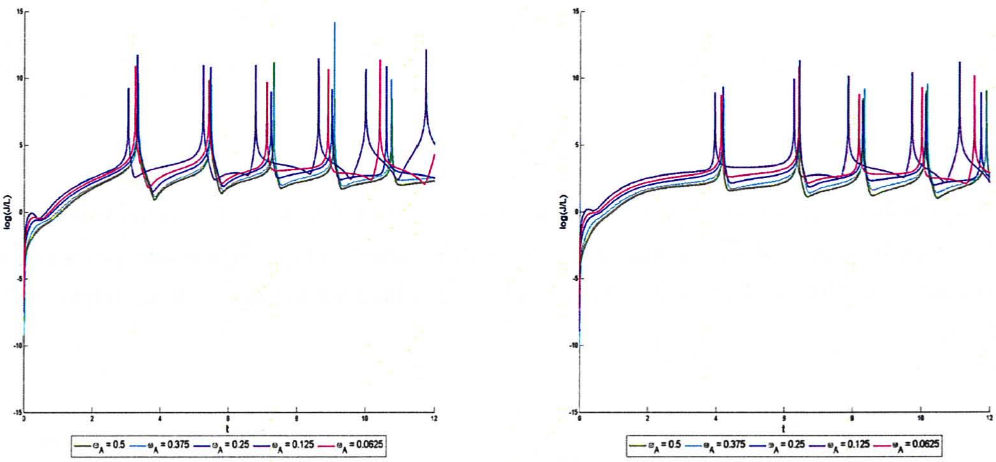

Figure 5.6: Ratio of the Mean of the magnetic helicity flux to the mean of the angular momentum flux for $\kappa = 1.5$ (top left), $\kappa = 1.0$ (top right), $\kappa = 0.75$ (lower left), $\kappa = 0.5$ (lower left). Since the parameters lie outside of the asymptotic regime there is little to no growth in these modes.

Bibliography

Balbus, S. A. & Hawley, J. F. 1991, ApJ, 376, 214

Balbus, S. A., Hawley, J. F., & Stone, J. M. 1996, ApJ, 467, 76

Biskamp, D. 1993, Nonlinear magnetohydrodynamics, ed. Biskamp, D.

Chandrasekhar, S. 1960, Proceedings of the National Academy of Science, 46, 253

Chorin, A. J. 1967, Journal of Computational Physics, 2, 12

Chorin, A. J. & Marsden, J. E. 1979, A mathematical introduction to fluid mechnanics, ed. Chorin, A. J. & Marsden, J. E.

Frisch, U. & Orszag, S. A. 1990, Physics Today, 43, 24

Lynden-Bell, D. & Pringle, J. E. 1974, MNRAS, 168, 603

Parker, E. N. 1970, ApJ, 162, 665

Shakura, N. I. & Sunyaev, R. A. 1973, A&A, 24, 337

Tout, C. A. & Pringle, J. E. 1992, MNRAS, 259, 604

Velikhov, E. P. 1959, Journal of Theoretical and Experimental Physics (U.S.S.R), 36, 1398

Vishniac, E. T. 2009, ApJ, 696, 1021

Vishniac, E. T. & Cho, J. 2001, ApJ, 550, 752

Vishniac, E. T. & Diamond, P. 1992, ApJ, 398, 561